Multi-fidelity model assessment of climate change impacts on river water temperatures, thermal extremes and potential effects on cold water fish in Switzerland

Love Råman Vinnå¹, Vidushi Bigler², Oliver S. Schilling^{3,4}, Jannis Epting^{*1}

OrcIDs:

Love Råman Vinnå: https://orcid.org/0000-0002-9108-8057

Jannis Epting: https://orcid.org/0000-0001-9578-5557

Oliver S. Schilling: https://orcid.org/0000-0003-3840-7087

¹Applied and Environmental Geology, Hydrogeology, Department of Environmental Sciences, University of Basel, CH-4056 Basel, Switzerland

²Bern University of Applied Sciences, Engineering and Computer Science (BFH-TI), Institute for Optimization and Data Analysis (IODA), 2501 Biel, Switzerland

³Hydrogeology, Department of Environmental Sciences, University of Basel, CH-4056 Basel, Switzerland

⁴Department Water Resources and Drinking Water, Eawag - Swiss Federal Institute of Aquatic Science and Technology, CH-8600 Dübendorf, Switzerland

^{*}Corresponding author: jannis.epting@unibas.ch

Abstract

River water temperature is a key factor for water quality, aquatic life, and human use. Under climate change, inland water temperatures have increased and are expected to do so further, increasing the pressure on aquatic life and reducing the potential for human use. Here, future river water temperatures are projected for Switzerland based on a multi-fidelity modeling approach. We use 2 different, semi-empirical surface water temperature models, 22 coupled and downscaled general circulation- to regional climate models, future projections of river discharge from 4 hydrological models and 3 climate change scenarios (RCP2.6, 4.5, and 8.5). By grouping catchments under representative thermal regimes, and by employing hierarchical cluster-based thermal pattern recognition, an optimal model and model configuration was selected, thereby improving model performance.

Results show that, until the end of the 21st century, average river water temperatures in Switzerland will likely increase by 3.2±0.7 °C (or 0.36±0.1 °C per decade) under RCP8.5, while under RCP2.6 the temperature increase may remain at 0.9±0.3 °C (0.12±0.1 °C per decade). Under RCP8.5, temperatures of rivers classified as being in the *Alpine* thermal regime will increase the most, that is, by 3.5±0.5 °C, followed by rivers of the *Downstream Lake* regime, which will increase by 3.4±0.5 °C. Under RCP2.6 temperatures in the Alpine and Downstream lake regimes change most with +1.15 and +0.99±0.5 °C.

A general decrease of river discharge in summer (-10 to -40 %) and increase in winter (+10 to +30%), combined with a further increase in average near-surface air temperatures (0.5 °C per decade), bears the potential to not only result in overall warmer rivers, but also in prolonged periods of extreme summer river water temperatures. This dramatically increases the thermal stress potential for temperature sensitive aquatic species such as the brown trout in rivers where such periods occur already, but also in rivers where this previously was not a problem. By providing information on future water temperatures, the results of this study can guide management's climate mitigation efforts.

1 Introduction

River water temperature is a key factor in the regulation of physical and biogeochemical processes in aquatic systems, affecting water quality, aquatic life and the potential for human water use. Globally, climate change has already increased, and is expected to further increase, river water temperatures (Van Vliet et al., 2011; 2013). Without climate protection, it is estimated that, globally, 36% of fish species will see their future habitats exposed to climate extremes, with changes in water temperatures being deemed more critical than the change in water availability (Barbarossa et al., 2021). The amount of river warming, especially during heat waves and droughts, is however not only a function of near-surface air temperatures, but also of river discharge, river-groundwater interactions, and human activities such as channelization, damming, water use for cooling purposes, or sewage and storm water runoff all affecting water quality (Ficklin et al., 2023; Van Vliet et al., 2023).

In Switzerland, the water tower of Europe, the effects of a changing climate have already influenced both river temperatures (Hari & Güttinger, 2004) and river discharge (Birsan et al., 2005). According to the latest regional climate projections (CH2018, 2018) the change is likely to continue to affect Swiss waterbodies in the future (FOEN, 2021). Past water temperature trends in Switzerland from 1979 to 2018 amounted to an increase of 0.33 °C per decade on average, alongside a near-surface air temperature increase of 0.46 °C per decade (Michel et al., 2020). Using a limited subset of federally monitored Swiss catchments (~10%) and a high emission climate scenario (RCP8.5), it was projected that water temperatures may continue to increase by 3.5 °C until the end of the 21st century (Michel et al., 2022). Being a higher elevation country (mean elevation 1,350 m asl), most rivers in Switzerland are populated by the brown trout (salmo trutta fario), a cold-water fish (Brodersen et al., 2023). All fish species have specific temperature limits within which optimal conditions for growth, health, reproduction, or life, exist. For the brown trout, which is a particularly temperature sensitive fish species, warmer water temperatures of around 13°C pose a threat for egg survival, 15 °C strongly increases their receptivity for parasites related illnesses, and prolonged exposure to 25°C can lead to death (Strepparava et al., 2018; Wehrly et al., 2007; Chilmonczyk et al., 2002; Elliott, 1994). A prime example of a water temperature related threat is the elevation (i.e., water temperature) dependent proliferative kidney disease (PKD), a parasite-caused illness in brown trout which is increasingly wide-spread in Swiss catchments (Hari et al., 2006).

A common challenge for model-based studies is the question of the optimal model to use. In surface hydrological applications, models can broadly be split into two major groups: processbased and statistical/stochastic models (Benyahya et al., 2007). Process-based models are based on physical equations and can resolve many hydrological processes in a physically robust manner, from the local to the catchment scale. However, albeit physically more robust, processbased models generally require a significant amount of input data and computational resources for the simulation of hydrological processes on the catchment scale, therefore limiting their applicability for climate change analyses on national scales. Statistical/stochastic models, as opposed to process-based models, are data driven, that is, are based on empirical relationships between input and output data. While they are physically less robust, their advantage lies in their relative simplicity and limited data requirements, sacrificing detail for increased repeatability and spatial coverage. However, in order to build on the efficiency of statistics whilst preserving a clear physical basis, as a compromise between the two major model groups, a sub-group of semi-empirical models, which employs physically meaningful equations but simplifies the more complex processes into purely empirical parameters, was developed (Piccolroaz et al., 2013). These semi-empirical models are ideally suited for hydrological climate change projections, as they provide much more robust projections compared to purely statistical approaches but simultaneously allow for a more comprehensive analysis than process-based models by enabling multi-model climate change ensemble analyses (La Fuente et al., 2022; Meehl et al., 2007).

The study of climate change includes the investigation of physical processes on global, regional and local scales. As scales change so too does the required level of detail needed to resolve the different water cycle components that are relevant on the respective scale. An ideally suited approach to address this challenge in hydrological modeling is a multi-fidelity model framework, which combines multiple computational models of varying complexity in an automated selection framework that ensures robust predictions while limiting the computation to only the necessary level of detail (Fernández-Godino, 2023). The use of process dependent fidelity ensures proper representation of physical processes on regional to local scales while keeping computational costs to a minimum. Multi-fidelity modeling is especially useful when acquiring high-accuracy data is costly and/or computationally intensive, as is the case for climate change impact assessment on the hydrological cycle.

Given the past and future changes to Swiss river water temperatures and considering both the high sensitivity of aquatic species to river water temperatures and the increasing demand for river water by agriculture, industry and society as a whole, it is critical to obtain a robust spatial and temporal understanding of the temperature increases that are expected for the many different rivers and streams of Switzerland. Here, we developed an efficient multi-fidelity modeling method guided by statistical pattern recognition to estimate river water temperatures under climate change and thereby close the aforementioned spatial gap by determining, in an automated manner and on a national scale, how future river water temperatures are likely going to change. Compared to previous projections of climate warming in Swiss rivers (Michel et al., 2022), the simplified multi-fidelity modeling approach not only enabled to cover the national scale (+90%) but also further thermal regimes (here 5, previously 2) and based on 22 GCM-RCM chains (previously 7). By grouping catchments together via statistical pattern recognition, we were able to classify rivers (including spring-fed rivers) into 5 different thermal regimes, improving model results by allowing for optimal model selection at each station and enabling regime-specific analyses. The effect on warming by changing river discharge was investigate through a hysteresis analysis. Additionally, we introduce the extreme event severity index as an analytic tool to evaluate the change in thermal extreme amplitude.

2 Materials & Methods

In climate change studies of the hydrosphere, unknown biases present a fundamental challenge. These biases can arise from limitations in how well models capture future physical processes, as well as from assumptions embedded in climate scenarios. To limit the influence of unknown bias, a common method is the multi-fidelity modeling approach which combines multiple models with different processes of fidelity. Using multiple models (as well as climate scenarios), while accepting that process-specific model performance differs from model to model, minimizes the risk of large bias towards the real future through a widening of the range of projections being made. Advantages for hydrological studies include the improvement of robustness of low-flow forecasts and accountability of structural uncertainty (Nicolle et al., 2020). As such, the method has been used to limit the uncertainty caused by hydrological models on runoff and evaporation climate projections using large ensembles of global hydrological models while investigating regional and global water scarcity in the future (Schewe et al., 2014). Even though varying model fidelity with varying complexity and

computational constraints is an advantage to hydrological modeling, care is needed when adding processes depending on the relevance of the process in the local area under investigation (Guse et al., 2021).

In this study a multi-fidelity modeling approach using two semi-empirical surface water temperature models, air2water and air2stream (Toffolon & Piccolroaz, 2015; Piccolroaz et al., 2013), was employed. This allowed limiting the computational requirements to the levels needed for climate change ensemble simulations. All available model configurations (i.e., 3, 4, 5, 6, 7 and 8 different parameter combinations and implementations) were evaluated for their applicability to different thermal river regimes (Appendix A) and allowed for developing optimal site-specific models for all the 82 thermal river monitoring stations of the Swiss Federal Office of the Environment (FOEN).

As the driving model forcing (i.e., hydrological boundary conditions), we used downscaled near-surface air temperature projections from 22 coupled general circulation to regional climate models (GCM-RCM) from 9 GCM and 8 RCM, and combined them with projections of future stream discharge from 4 hydrological models for 3 climate change scenarios (i.e., representative concentration pathways) representing all climate protection measures with RCP2.6, moderate measures by RCP4.5, and business as usual by RCP8.5. Following recommendations from the Word Meteorological Organization (WMO, 2017) to use 30 years of continuous data while evaluating climate change, we selected 3 periods of interest including a reference period (1990 to 2019) and both a near- (2030 to 2059) and far-future period (2070 to 2099). The method pathway is visualized in Figure 1.

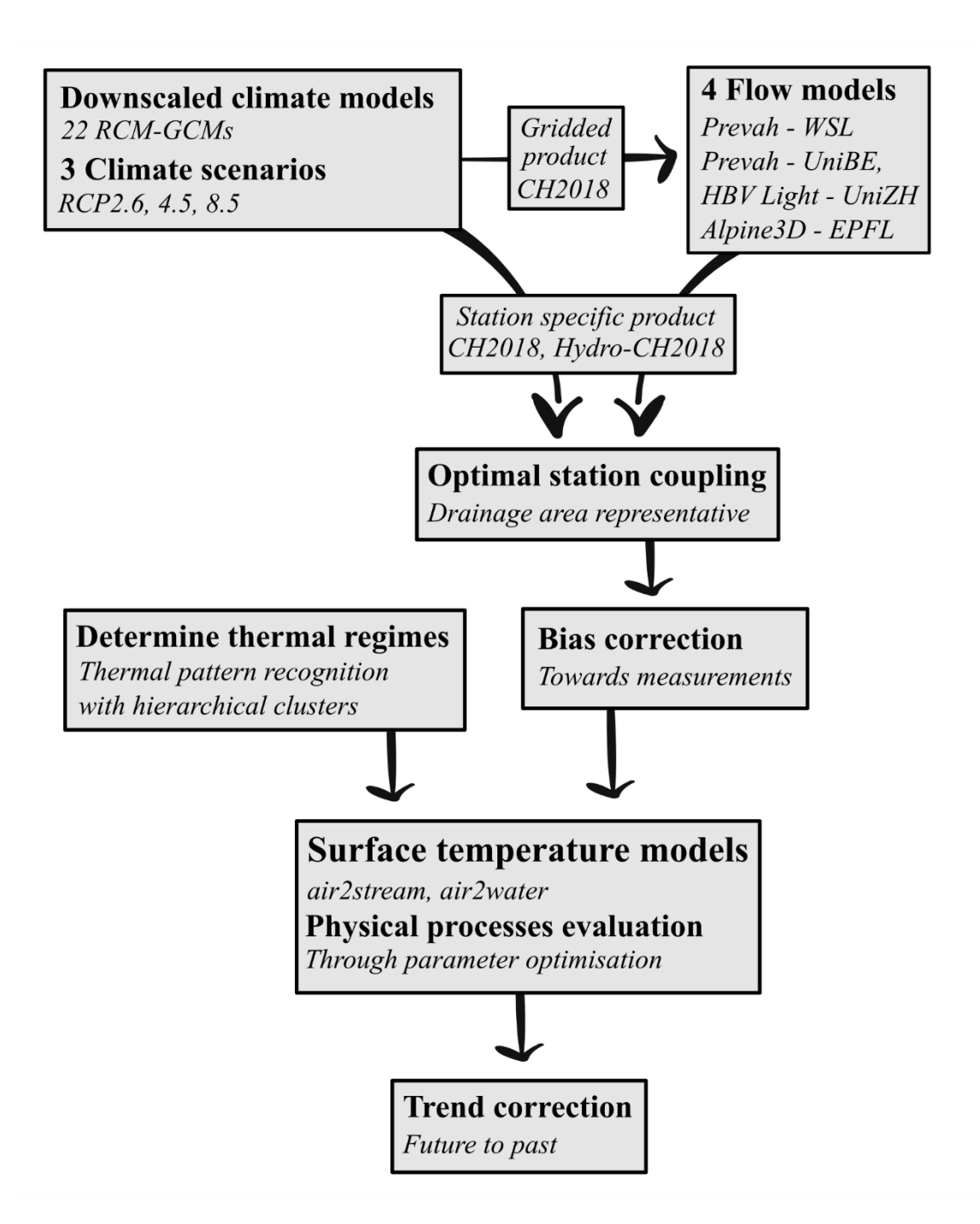


Figure 1. Workflow summarizing the data treatment and the multi-fidelity model selection and optimization.

2.1 Data

River water temperatures are directly influenced by both global and, to an even greater extent, local conditions in and above the drainage area, especially in regions divided by geographic barriers such as mountains (Ficklin et al., 2023). To analyze site-specific controls and project future river water temperatures, measured historic and simulated future climate data should thus be representative of the conditions and hydrologic processes upstream of the locations to be studied. The air2stream and air2water models require both measured historic and simulated future climate data to extend to at least a year (ideally more than one) and be daily resolved. However, to be sure that the effect of climate is included in calibration and analysis of future conditions, data should preferably cover 30 years (WMO, 2017; Piccolroaz et al., 2013).

Temporally overlapping, daily averaged near-surface air temperature and river discharge measurements spanning the 30-year reference period of 1990 to 2020 were used as calibration data, while for validation the data from 1980 to 1990 were used (Table B2 in Appendix). By choosing to use the most recent data for calibration rather than validation ensures that recent

local climate conditions are carried into future projections (Shen et al., 2022). For the few cases where no forcing data for calibration did exist between 1990 to 2020 (Table B2), validation was deprioritized and calibration performed for the 1980-1990 data.

Here we use CH2018 climate simulations based on the EURO-CORDEX regional climate modeling ensemble. In CH2018 near-surface air temperatures was downscaled by applying a statistical bias-correction and downscaling method (Quantile Mapping, a purely statistical and data-driven method) to the original output of all EURO-CORDEX climate model simulations, as observational reference station observations and observation-based gridded analyses were used (CH2018, 2018, Chapter 5). These data are available as both gridded and local station products (CH2018 Project Team, 2018). Following CH2018, the Hydro-CH2018 project analyzed the effects of climate change on Swiss water bodies (FOEN, 2021). The gridded climate product from CH2018 was used to construct projections of future river discharge for 4 hydrological models used in Hydro-CH2018. The location where output from these 4 models was used in this study is shown in Figure 2a including: (M₁) PREVAH-WSL a conceptual process-based model (Brunner, et al., 2019a; Brunner, et al., 2019b) and (M2) PREVAH-UniBE (Muelchi et al., 2021), (M₃) HBV Light-UniZH a bucket-type hydrological model (Freudiger et al., 2021), and (M₄) AlpineFlow-EPFL the snowmelt and runoff model Alpine3D coupled to the semi-distributed hydrological model StreamFlow (Michel et al., 2022). The Hydro-CH2018 project produced projections for 61 out of the 82 FOEN river monitoring stations under 22 GCM-RCM model chains (9 GCM coupled to 8 RCM runs) with 0.11° and 0.44° resolution and 3 climate change scenarios (RCP2.6, 4.5, and 8.5). The available projections, the employed circulation and hydrological models, and the considered climate change scenarios for all the different stations that were considered in this study are summarized in Table 1.

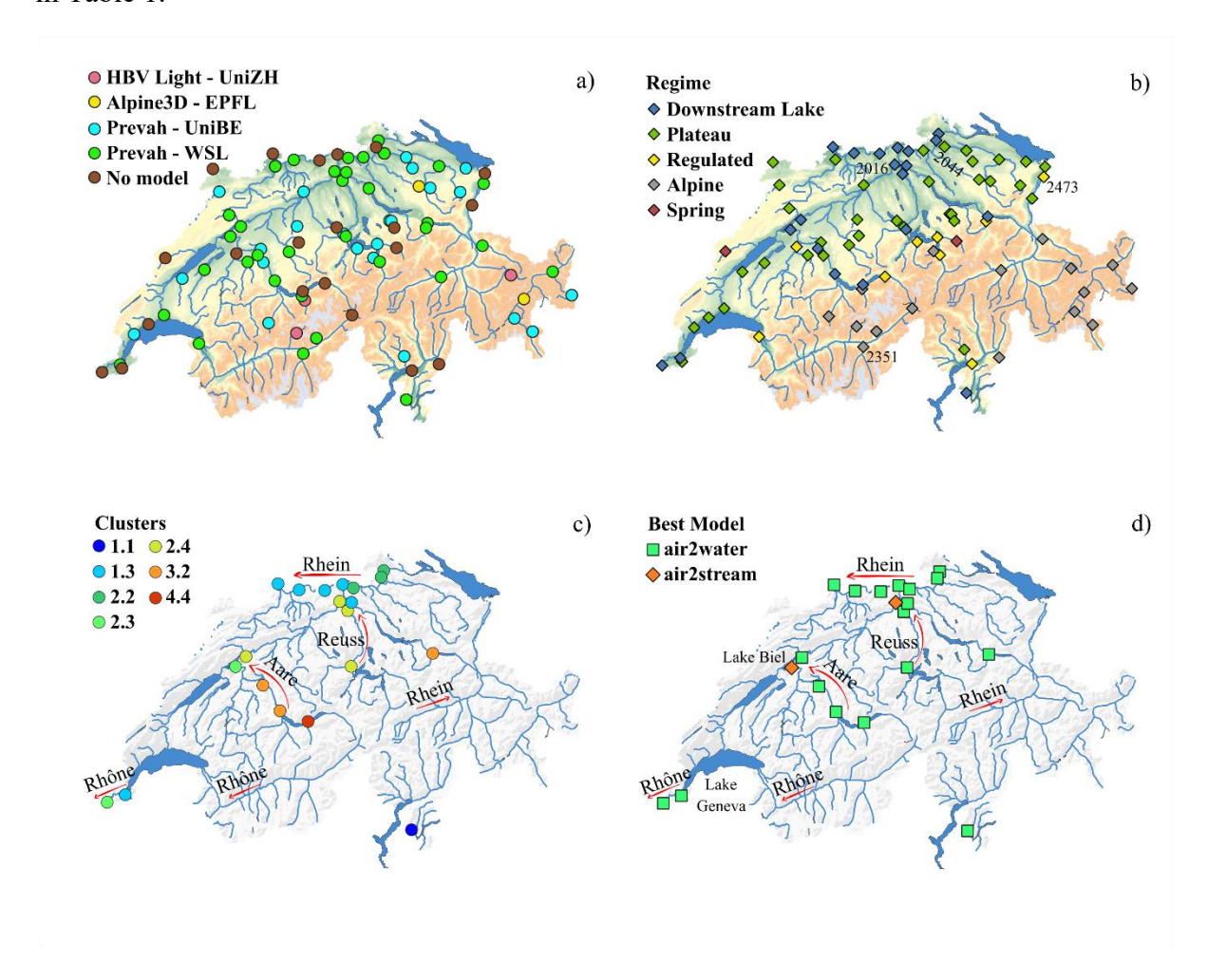


Figure 2. a) Investigated FOEN stations with available and used hydrological models providing future projections of river flow, b) station thermal regimes, c) downstream lake clusters, d) best performing surface water temperature model at downstream lake stations. Red arrows show river flow directions. Coordinate reference system is the Swiss LV95. Background map is the DHM25, swisstopo.admin.ch/de/geodata/height/dhm25.html).

From models M₁-M₃, continuous projections of river discharge at daily resolution for the entire period covering 1990-2099 were available, projections from the M₄ model were discontinuous and only covered the periods 1990-2000, 2005-2015, 2030-2040, 2055-2065, and 2080-2090, respectively. River temperature simulations of river monitoring stations for which forcing data from models M₁-M₃ were available covered the entire period of 1990-2099, while for stations for which only data from model M₄ were available, simulations were only run for the periods for which data was available.

Measurements of historic meteorologic and hydraulic parameters which were used for model calibration, validation and for bias correction were obtained at daily resolution from the MeteoSwiss IDAweb platform (meteoschweiz.admin.ch) and from the Hydrology Division of the Federal Office for the Environment FOEN (hydrodaten.admin.ch). For monitoring stations at which historic river discharge data or future river discharge projections were not available, only future near-surface air temperature projections were used to simulate water temperature. Where climate projections were available at multiple different spatial resolutions (i.e. 0.11° and 0.44°), only one model, as indicated in Table 1, was included in the analysis, following the approach of Muelchi et al., 2021.

Table 1. Climate projections and hydrological models used for temperature simulation. For a complete climate model designation, see the CH2018 project report (CH2018, 2018). Models analyzed are indicated by an "X" mark, and models not analyzed but with simulation data provided by a "(X)" mark.

GCM	RCM	PREVAH-WSL (M ₁)					PREVAH-UniBE (M2)						
		RC	P8.5	RC	P4.5	RC	P2.6	RCP	8.5	RC	P4.5	RC	P2.6
		0.11°	0.44°	0.11°	0.44°	0.11°	0.44°	0.11°	0.44°	0.11°	0.44°	0.11°	0.44°
	KNMI-RACMO22E		X		X				X		X		
	DMI-HIRHAM5	X	(X)	X	(X)	X	(X)	X	(X)	X	(X)	X	
ICHEC-EC-EARTH	CLMcom-CCLM4-8-17							X		X			
	CLMcom-CCLM5-0-6		X						X				
	SMHI-RCA4	X	(X)	X	(X)	X	(X)	X	(X)	X	(X)	X	(X)
	CLMcom-CCLM4-8-17		X					X	(X)	X			
MOHC-HadGEM2-ES	CLMcom-CCLM5-0-6		X						X				
	ICTP-RegCM4-3												
	KNMI-RACMO22E		X		X		X		X		X		X
	SMHI-RCA4	X	(X)	X	(X)		X	X	(X)	X	(X)		X
	CLMcom-CCLM4-8-17							X	(X)	X	(X)		
	CLMcom-CCLM5-0-6		X						X				
MPI-M-MPI-ESM-LR	MPI-CSC-REMO2009-1							X	(X)	X	(X)	X	(X)
	SMHI-RCA4	X	(X)	X	(X)		X	X	(X)	X	(X)		X
	MPI-CSC-REMO2009-2							X	(X)	X	(X)	X	(X)
MIROC-MIROC5	CLMcom-CCLM5-0-6		X						X				
WIROC-WIROC3	SMHI-RCA4		X		X		X		X		X		X
CCCma-CanESM2	SMHI-RCA4		X		X				X		X		
CSIRO-QCCCE-CSIRO-Mk3-6-0	SMHI-RCA4								X		X		
IPSL-IPSL-CM5A-MR	SMHI-RCA4		•	,	•	•	, and the second	X	(X)	X	(X)	•	
NCC-NorESM1-M	SMHI-RCA4		X		X		X		X		X		X
NOAA-GFDL-GFDL-ESM2M	SMHI-RCA4								X		X		

GCM	RCM	RCM HBV Light-UniZH (M ₃)					AlpineFlow-EPFL (M4)						
		RCP8.5		RCP4.5		RCP2.6		RCP8.5		RCP4.5		RCP2.6	
		0.11°	0.44°	0.11°	0.44°	0.11°	0.44°	0.11°	0.44°	0.11°	0.44°	0.11°	0.44°
	KNMI-RACMO22E		X		X								
ICHEC-EC-EARTH	DMI-HIRHAM5	X		X		X		X		X		X	
	CLMcom-CCLM4-8-17	X		X									
	CLMcom-CCLM5-0-6		X										
	SMHI-RCA4	X		X		X		X		X		X	
	CLMcom-CCLM4-8-17	X		X									
MOHC-HadGEM2-ES	CLMcom-CCLM5-0-6		X										
	ICTP-RegCM4-3		X										
	KNMI-RACMO22E		X		X		X		X		X		X
	SMHI-RCA4	X		X			X		X		X		X
	CLMcom-CCLM4-8-17	X		X									
	CLMcom-CCLM5-0-6		X										
MPI-M-MPI-ESM-LR	MPI-CSC-REMO2009-1												
	SMHI-RCA4	X		X			X		X		X		X
	MPI-CSC-REMO2009-2	X		X		X							
MIROC-MIROC5	CLMcom-CCLM5-0-6		X										
MIROC-MIROC3	SMHI-RCA4		X		X		X		X		X		X
CCCma-CanESM2	SMHI-RCA4		X		X								
CSIRO-QCCCE-CSIRO-Mk3-6-0	SMHI-RCA4		X		X								
IPSL-IPSL-CM5A-MR	SMHI-RCA4	X		X									
NCC-NorESM1-M	SMHI-RCA4		X		X		X		X		X		X
NOAA-GFDL-GFDL-ESM2M	SMHI-RCA4		X	-	X								

GCM	RCM	No Flow Projection							
		RC	P8.5	RCP4.5		RC	P2.6		
		0.11°	0.44°	0.11°	0.44°	0.11°	0.44°		
	KNMI-RACMO22E		X		X				
	DMI-HIRHAM5	X	(X)	X	(X)	X			
ICHEC-EC-EARTH	CLMcom-CCLM4-8-17	X		X					
	CLMcom-CCLM5-0-6		X						
	SMHI-RCA4	X	(X)	X	(X)	X	(X)		
	CLMcom-CCLM4-8-17	X	(X)	X					
	CLMcom-CCLM5-0-6		X						
MOHC-HadGEM2-ES	ICTP-RegCM4-3		X						
	KNMI-RACMO22E		X		X		X		
	SMHI-RCA4	X	(X)	X	(X)		X		
	CLMcom-CCLM4-8-17	X	(X)	X	(X)				
	CLMcom-CCLM5-0-6		X						
MPI-M-MPI-ESM-LR	MPI-CSC-REMO2009-1	X	(X)	X	(X)	X	(X)		
	SMHI-RCA4	X	(X)	X	(X)		X		
	MPI-CSC-REMO2009-2	X	(X)	X	(X)	X	(X)		
MIROC-MIROC5	CLMcom-CCLM5-0-6		X						
WIROC-WIROC3	SMHI-RCA4		X		X		X		
CCCma-CanESM2	SMHI-RCA4		X		X				
CSIRO-QCCCE-CSIRO-Mk3-6-0	SMHI-RCA4		X		X				
IPSL-IPSL-CM5A-MR	SMHI-RCA4	X	(X)	X	(X)				
NCC-NorESM1-M	SMHI-RCA4		X		X		X		
NOAA-GFDL-GFDL-ESM2M	SMHI-RCA4		X		X		•		

2.2 Hydrologic and meteorologic station coupling

Switzerland is characterized by a pronounced topography. Therefore, the closest meteorological station to a hydraulic station might not necessarily be the ideal coupling partner. Hydrological and meteorological stations therefore were paired according to the following procedure: Only stations were considered for which (a) future climate projections of nearsurface air temperatures (required) and river discharge (optional, but desirable for improved water temperature predictions) were available for the entire period covering 1980 to 2099, and (b) historic measurements of near-surface air temperatures and river discharge were available from 1980 to 2020. Meteorological stations were subsequently paired with hydrological stations such that (a) the horizontal distance between river and meteorological stations was as small as possible i.e. nearest to nearest (criterion DIS), (b) the meteorological station was representative for the conditions in the upstream drainage area composing a meteorological station being located in the same valley and upstream (criterion DRA), and (c) the elevation difference did not exceed a reasonable threshold of 200 m (criterion ELE). Where possible, all three criteria were met, that is the closest station passed both *ELE* and *DRA* and are noted as DIS in Table 2. If the closest station were deemed not to be representative (e.g. in a neighboring valley or downstream) the DIS criteria where failed, such a station are noted as DRA in Table 2. If a station failed both DIS and DRA but passed ELE it is noted as ELE in Table 2. Station details and pairings are summarized in Table 2.

Table 2. Combined river and meteorological stations and available models for climate projections of discharge. Abbreviations: *DIS*: Distance; *ELE*: Elevation; *DRA*: Drainage area.

FOEN Hydrological stations					Meteorological stations					gical m	nodels
Name	ID	Height	Area	Acronym	Height	Distance	Criteria	Hydrological mod Hydro-CH2018			
DIA D 4 1 C	2000	(m asl)	(km²	AIC	(m asl)	(km)	DIC	M_1	M_2	M_3	M_4
Rhône - Porte du Scex Aare - Brugg	2009 2016	377 332	5238 1168	AIG BUS	381 387	3.8 14.0	DIS DIS	X X			
Reuss - Mellingen	2018	345	3386	BUS	387	15.0	DIS	X			
Aare - Brienzwiler	2019	570	555	MER	588	6.1	DIS				
Aare - Brügg, Aegerten	2029	428	8249	BER	553	20.0	ELE	X			
Aare - Thun	2030	548	2459	INT	577 556	22.3	DIS	X	v		
Vorderrhein - Ilanz Broye - Payerne, Caserne d'aviation	2033 2034	693 441	774 416	CHU Pay	490	26.9 2.7	DRA DIS	X	X X		X
Thur - Andelfingen	2044	356	1702	SHA	438	11.4	DIS	X	X	X	21
Reuss - Seedorf	2056	438	833	ALT	438	0.4	DIS	X	X		
Ticino - Riazzino	2068	200	1613	MAG	203	1.8	DIS				
Emme - Emmenmatt, nur Hauptstation	2070	638	443	LAG	744	4.7	DIS	X	X X		
Muota - Ingenbohl Aare - Hagneck	2084 2085	438 437	317 5112	ALT BER	438 553	12.8 22.5	DIS DRA	X	Λ		
Rhein - Rheinfelden, Messstation	2091	262	3452	BAS	316	16.4	DIS	X			
Linth - Weesen, Biäsche	2104	419	1062	GLA	517	10.9	DIS	X	X		
Birs - Münchenstein, Hofmatt	2106	268	887	BAS	316	3.7	DIS	X	X	**	X
Lütschine - Gsteig	2109 2112	585 769	381 74.4	INT STG	577 776	0.9 10.4	DIS DIS	X	X	X	X
Sitter - Appenzell Aare - Felsenau, K.W. Klingnau (U.W.)	2112	312	1768	BUS	386	25.8	DRA		Λ		
Murg - Wängi	2126	466	80.2	TAE	539	4.1	DIS		X		
Rhein (Oberwasser) - Laufenburg	2130	299	3405	RUE	611	18.6	DIS				
Aare - Bern, Schönau	2135	502	2941	BER	553	6.5	DIS	X			
Rheintaler Binnenkanal - St. Margrethen	2139 2143	404 323	175 1476	VAD	457 426	37.3 18.5	DRA	v			
Rhein - Rekingen Landquart - Felsenbach	2143	523 571	614	KLO RAG	426 497	18.5 9.5	DRA DIS	X			
Reuss - Luzern, Geissmattbrücke	2152	432	2254	LUZ	454	2.0	DIS	X			
Gürbe - Belp, Mülimatt	2159	522	116.0	BER	553	12.1	DIS		X		
Massa - Blatten bei Naters	2161	1446	196	GRC	1605	24.9	ELE	X		X	
Tresa - Ponte Tresa, Rocchetta	2167	268	609	LUG	273	9.1	DIS	X	X		
Arve - Genève, Bout du Monde Rhône - Chancy, Aux Ripes	2170 2174	380 336	1973 1030	GVE GVE	410 411	7.9 16.0	DIS DIS				
Sihl - Zürich, Sihlhölzli	2174	412	343	SMA	556	3.2	DIS	X	X		
Sense - Thörishaus, Sensematt	2179	553	351	BER	553	14.3	DIS	X	X		
Thur - Halden	2181	456	1085	GUT	440	11.8	DIS	X	X		
Doubs - Ocourt	2210	417	1275	FAH	596	13.0	DIS		X		
Allenbach - Adelboden	2232 2243	1297	28.8	ABO	1321 444	0.9	DIS	X	X		
Limmat - Baden, Limmatpromenade Rosegbach - Pontresina	2243	351 1766	2384 66.5	REH SAM	1709	16.6 4.3	DIS DIS	Λ	X		
Inn - Tarasp	2265	1183	1581	SCU	1304	0.6	DIS	X			
Lonza - Blatten	2269	1520	77.4	GRC	1605	24.9	ELE			X	X
Grosstalbach - Isenthal	2276	767	43.9	ALT	438	5.3	DIS		X	X	
Sperbelgraben - Wasen, Kurzeneialp	2282	911	0.56	NAP	1403	7.5	DIS	v			
Rhein - Neuhausen, Flurlingerbrücke Areuse - St-Sulpice	2288 2290	383 755	1193 104	SHA BRL	438 1050	0.9 9.0	DIS DRA	X			
Suze - Sonceboz	2307	642	127	CHA	1594	11.5	DIS	X	X		X
Goldach - Goldach, Bleiche, nur Hauptstation	2308	399	50.4	GUT	440	19.3	ELE		X		
Dischmabach - Davos, Kriegsmatte	2327	1668	42.9	DAV	1594	4.9	DIS			X	X
Langeten - Huttwil, Häberenbad	2343	597	59.9	WYN	422	15.0	DIS		X		
Riale di Roggiasca - Roveredo, Bacino di Vispa - Visp	2347 2351	980 659	8.12 786	GRO VIS	323 639	6.0 3.6	DIS DIS	X			
Poschiavino - La Rösa	2366	1860	14.1	BEH	2260	3.8	DIS	Λ	X	X	
Mentue - Yvonand, La Mauguettaz	2369	449	105.0	PAY	490	17.1	ELE		X	21	
Linth - Mollis, Linthbrücke	2372	436	600	GLA	517	7.4	DIS	X	X		
Necker - Mogelsberg, Aachsäge	2374	606	88.1	EBK	623	10.1	DIS		X		
Murg - Frauenfeld	2386	390	213	TAE SHA	539	9.9	DIS		X		
Rhein (Oberwasser) - Rheinau Liechtensteiner Binnenkanal - Ruggell	2392 2410	353 435	1195 116	VAD	438 457	5.8 12.9	DIS DIS				
Rietholzbach - Mosnang, Rietholz	2414	682	3.19	EBK	623	13.5	DIS				X
Glatt - Rheinsfelden	2415	336	417	KLO	426	11.4	DIS	X	X		
Venoge - Ecublens, Les Bois	2432	383	228.0	PUY	456	9.2	DIS	X	X		
Aubonne - Allaman, Le Coulet	2433	390	105	CGI	458 422	15.9	DIS		X		
Dünnern - Olten, Hammermühle Aare - Ringgenberg, Goldswil	2434 2457	400 564	234 1138	WYN INT	577	13.3 2.5	DRA DIS		Λ		
Inn - S-Chanf	2462	1645	616	SAM	1708	13.3	DIS				X
Saane - Gümmenen	2467	473	1881	BER	552	17.6	DIS				
Rhein - Diepoldsau, Rietbrücke	2473	410	6299	VAD	457	29.9	DRA	X			
Engelberger Aa - Buochs, Flugplatz	2481	443	228	LUZ	454	10.6	DIS		X	X	
Allaine - Boncourt, Frontière	2485	366	212	FAH	596	10.1	DIS		v		
Promenthouse - Gland, Route Suisse Schlichenden Brünnen - Muotathal	2493 2499	394 638	120 31	CGI ALT	458 437	3.2 15.6	DIS DIS		X		
Worble - Ittigen	2500	522	67.1	BER	553	2.2	DIS		X		
Biber - Biberbrugg	2604	825	31.9	EIN	911	3.5	DIS		X		
Rhône - Genève, Halle de l'île	2606	367	8000	GVE	411	4.9	DIS	X			
Sellenbodenbach - Neuenkirch	2608	515	10.4	LUZ	454	11.0	DIS		v		
Alp - Einsiedeln Riale di Pincascia - Lavertezzo	2609 2612	840 536	46.7 44.5	EIN OTL	911 367	2.4 10.4	DIS ELE		X X		
Rhein - Weil, Palmrainbrücke	2612	244	3645	BAS	316	6.7	DIS		Λ		
Rom - Müstair	2617	1236	128	SMM	1386	0.4	DIS		X	X	
Rhône - Oberwald	2623	1368	93.3	ULR	1345	4.6	DRA				
Kleine Emme - Emmen	2634	430	478	LUZ	454	4.2	DIS		X	X	X
Grossbach - Einsiedeln, Gross	2635	942	8.95	EIN	910	3.0	DIS	<u> </u>			

2.3 Forcing data bias correction

Differences between near-surface air temperature measurements used for calibration and climate model projections, even when slight, may artificially alter the quantification of projected future river water temperatures by introducing a systematic bias at the start of the simulations. Despite the fact that the highly resolved GCM-RCMs model output data that were considered were already statistically downscaled, small differences between modeled and observed air temperatures during the reference period could still be detected.

For the river discharge projections, no bias correction has so far been performed. To mitigate this bias, the time series of air temperatures and river discharge used as climate forcing data were statistically adjusted using the change factor method (Diaz-Nieto & Wilby, 2005; Minville et al., 2008). This method adjusts climate projections towards measurements by removing the climatological year (consisting of daily averages) from first the modeled data and then adding the corresponding climatological year from measurements according to Eq. 1, thereby correcting long-term and seasonal biases while maintaining individual climate model trends and stochastic variabilities.

$$Fn_i = (Fo_i - Co_i) + Cm_i \tag{1}$$

where Fn_i is the adjusted variable at time i, Fo_i is the future climate simulated time series of either air temperatures or river discharge at daily resolution, and Co_j and Cm_j are the climatological years of the climate simulated time-series and the historic measurements, respectively, at the day of year j corresponding to time i. The climatological years were smoothed using a 60-day window to remove the effect of possible pulse events, especially for discharge. Due to low flow conditions in some rivers, discharge in the rivers were never adjusted below the minimum observed flow.

2.4 Thermal regime classification

For the multi-fidelity modeling approach, the different river monitoring stations were reclassified into the 4 different thermal regimes that have previously been identified for Switzerland (Michel et al., 2020; Piccolroaz et al., 2016) as well as 1 additional thermal regime defined for the purpose of this study.

The existing thermal regimes are *Downstream Lake*, *Swiss Plateau*, *Alpine*, *Regulated*, while the *Spring* discharge regime was added to address the special thermal case of stations situated at the mouth of spring fed streams. *Downstream Lake* stations show a clear de-coupling between river temperature and river discharge, *Swiss Plateau* stations exhibit an annual flow cycle with minimal discharge in summer and strong interannual variability, *Alpine* stations show that both discharge and temperature are strongly influenced by snow and glacier melt, *Regulated* stations are fed by intermittent releases of large volumes of water from upstream reservoirs, and *Spring* stations located immediately downstream of springs and characterized by a nearly constant temperature signal decoupled from air temperature.

The already existing classifications from (Michel et al., 2020; Piccolroaz et al., 2016) and the suitability of the yet unclassified stations to be grouped under the different thermal regimes were first explored by evaluating the historic data and the locations visually (Figure 2b). Following this first visual classification, an automated thermal pattern recognition using hierarchical clusters via the cluster tool DTWARP_PER_33 (Bögli, 2020) was used (Figure 2c). Application of the thermal pattern recognition matched the visual pre-classification in most cases, but revealed that, for certain stations located far downstream of lakes, upstream lake

processes are still the dominant control for river water temperatures. Stations that were previously classified as not being part of the *Downstream Lake* regime were thus here reclassified as *Downstream Lake* according to the results of the thermal pattern recognition procedure.

2.5 Surface water temperature model setup

Two semi-empirical surface water temperature models were employed, the river water model air2stream (Toffolon & Piccolroaz, 2015)*1 and the lake water model air2water (Piccolroaz et al., 2013)*2, with the former being an extended version of the latter. Both, the air2stream and the air2water models combine the simplicity of stochastic models with accurate empirical representation of the relevant physical processes affecting water temperature. The models require near-surface air temperature as input to predict future river temperature, while discharge may optionally be incorporated in air2stream to further improve river temperature predictions.

Both models include up to eight parameters (a_1 to a_8) which are fitted towards measured data. Apart from the effect of air temperature on water temperature, the models additionally resolve the effect of river depth, discharge, thermal signals from tributaries, inverse stratification in lakes during winter, and seasonal cycles. Model complexity, i.e. how many processes are directly being resolved by the models or indirectly included through parameter estimation, can be varied by removal of one or more of the additional processes listed above, resulting in the use of 8, 7, 6, 5, 4 or 3 parameters. Depending on local conditions, model performance can be improved by the removal of processes which play a minor or insignificant role for water temperature. Where this simplification with removal of parameters was done (Table B2), removed processes plays a minor role for the simulation of water temperature as evident from decreased model performance while being included. For additional information about air2stream and air2water see Appendix A and Piccolroaz et al. (2013) and Toffolon & Piccolroaz (2015).

For the simulation of future river temperatures, a multi-fidelity modeling approach that identified the best water temperature model for each single river monitoring station was employed. The optimal model parameter configuration for each station was identified via a Monte-Carlo calibration process performed with the Crank Nicolson scheme (Crank & Nicolson, 1947), consisting of over 2,000 runs using Particle Swarm Optimization (Kennedy & Eberhart, 1995) with 500 particles. The Root Mean Square Error (RMSE) function was used as the objective function and combined with the *dotty-plots* quality check (S. Piccolroaz et al., 2013; Piccolroaz, 2016; Toffolon et al., 2014).

For stations missing either historical data or future projections of river discharge (brown markers, Figure 2a), discharge was not considered as forcing data and the *air2stream* model was reduced to a 3 or 5 parameter model, while no adaptation was required for *air2water* model as it does not simulate discharge. Datasets used for calibration and validation with data gaps shorter than 30 days were filled by linear interpolation, while for datasets with gaps exceeding 30 days only the longest continuous dataset was used.

All simulations (calibration, validation and climate runs) used a one-year period as a spin-up with the first year of forcing data repeated. Only the best performing river temperature model was considered for the follow-on climate runs. The final calibration and validation periods and

^{*1} github.com/marcotoffolon/air2stream

^{*2} github.com/marcotoffolon/air2water

the best performing parameter setups for each station are provided in Table B2 (Appendix B). As initial conditions for the stepwise climate simulations with model M₄, we used simulated temperatures from the latest prior simulated date, that is, for simulations between 2030 to 2040 we used temperature from end of 2015 as initial condition.

At *Downstream Lake* stations, multiple configurations of both water temperature models (*air2stream* and *air2water*) were tested through calibration, and only the best performing temperature model and parameter setup was kept (station thermal regimes as well as cluster results are shown in Figure 2 and provided in Table B1 in Appendix B). For the remaining stations not belonging to the *Downstream Lake* regime, river processes such as local flow variations and water depth dominate the water temperature development. For these stations, different model configurations of only the *air2stream* model were explored.

2.6 Trend correction

Empirical models generally predict less warming in the future compared to physically based models, the primary reason being underrepresentation of the thermal catchment memory, including snow and ice (Leach & Moore, 2019). To quantify how good the models *air2stream* and *air2water*, which both lack deterministic considerations of snow and ice melt, are able to recreate past trends, we compared trends from river water temperature measurements and corresponding modeled temperature trends between 1990 and 2019. On an annual basis, this comparison was possible for 25 out of 82 river stations, consisting of 9 *Downstream Lake*, 7 *Regulated*, 7 *Swiss Plateau*, 2 *Alpine*, and 0 *Spring* thermal regime river stations. Stations were selected with a 30 years of continuous data requirement in air and water temperature and river discharge. Only statistically significant trends (p < 0.05) were considered.

Both *air2stream* and *air2water* underestimate the annual temperature trend during the reference period on average by 0.14 and 0.11 °C per decade, respectively. For *air2stream*, the annual trend bias is smallest for the *Swiss Plateau* thermal regime (0.09 °C per decade) and largest in the *Alpine* thermal regime (0.17 °C per decade). Seasonally, the trend bias is largest from June to August and September to November, whereas, especially for *air2water*, the bias is small from December to February and March to May.

The divergence of both *air2stream* and *air2water* models from observed trends warrant a post simulation bias correction of simulated trends. The bias is river station dependent, making an individual correction at each station preferable (Tables B3 to B6 in Appendix B). However, only about 30% of the river stations investigated have long enough data sets (30 years) for individual correction. Therefore, we tied the seasonal trend bias correction to the thermal regime, thereby keeping the correction linked to local conditions. Note that no river station of the *Spring* thermal regime had enough data to allow for the trend bias correction. *Spring* river stations were therefore not trend bias corrected. As the trend bias correction is acting on climate simulations of river temperature stretching from 1990 to 2099, the bias correction had to be scaled towards how air temperature trends shift in the climate models. The scaling was designed such that it did not affect the bias correction during the reference period (1990 to 2019), while adjusting the correction towards how the air temperature trend (*TTair*) changes in the near- (2030 to 2059) and far-future (2070 to 2099). For this purpose, an adjustment factor *Fs* (-) was constructed from the mean climate models air temperature trends for each climate scenario. *Fs* is thus specific for each climate scenario, river station and season.

$$Fs_{i,s} = \frac{TTair_{i,s}}{TTair_{ref,s}} \tag{2}$$

Here $TTair_{i,s}$ is the mean of the air temperature trends from the climate models, which is changing for each season and with the reference, near- and far-future periods, $TTair_{ref,s}$ is the mean of the seasonal air temperature trend during the reference period, i is the number of days, and s denotes the season. The temporal gaps between 1990 to 2019, 2030 to 2059 and 2070 to 2099, during which the air temperature trends were calculated, were linearly filled with shape-preserving piecewise cubic interpolation resulting in a continuous $factor Fs_{i,s}$ from 1990 to 2099. $Fs_{i,s}$ varied from -2 to +3 depending on the season and climate scenario and was applied for simulations using discharge input from models M_1 to M_3 , while for simulations using M_4 , $Fs_{i,s}$ was set to 1 from 1990 to 2099 due to too short simulation time frames in M_4 (only one decade). With $Fs_{i,s}$, the seasonal and thermal regime dependent water temperature bias $Tb_{i,s}$ (regime dependent mean from Table C3 to C6 in Appendix C) is turned into the thermal regime and climate scenario dependent seasonal bias correction Bc_s (°C day-1)

$$Bc_{s} = \sum_{i=1}^{i=n} Fs_{i,s} * Tb_{i,s}$$
(3)

where n is the number of days since 1st of January 1990. Before adjusting the water temperature model output from 1990 to 2099, the seasonal Bc_s was combined into a continuous dataset Bc. To avoid a sharp shift in Bc between each season, a 3- to 5-day gap in between each season was smoothed with shape-preserving interpolation (Piecewise cubic Hermite interpolation, PCHIP; Matlab R2022a).

The trend adjustment applied here with Fs, Bc, and pre- and post-adjustment data is shown from one example station in Figure B1 (Appendix B). Pre- and post-trend correction for the difference in modeled and measured trends is summarized in Table B7 (Appendix B).

2.7 Thermal hysteresis

Hysteresis, wherein a dependent variable (water temperature or suspended sediments) can exhibit multiple values in response to a single value from the independent variable (discharge), is a common phenomenon in hydrology (Gharari & Razavi, 2018). Sediment transport hysteresis can be caused in rivers by emptying and refilling of sediment layers on the river bed (Tananaev, 2012) and through erosion on land as shown in the Alps with the contributing location (river bed or eroded area) determining the hysteresis loop shape and rotation direction (Misset et al., 2019). Stream temperature can also show hysteresis effects, example being a lag in the response to air temperature caused by ice-melt or reservoir release (Van Vliet et al., 2011; Webb & Nobilis, 1994).

We investigated past and future hysteresis loops between water temperatures (the dependent variable) and river discharge (the independent variable) using a versatile index (Zuecco index, Zuecco et al., 2016). The Zuecco index works through the computation of definite integrals on data in chosen intervals and was developed for hysteretic loops where the independent variable increases from its initial value, reaches a peak and then decreases. The index divides loops into classes depending on rotation direction (counter clockwise or clockwise), number of loops and loop sizes.

Here we use Zuecco Class I to IV (Figure 3, left column) which represent the interaction between flow and water temperature for the cases of dataset starting with low temperature and low flow. However, mainly in the Swiss lowland at the beginning of a year, rivers can display a situation where temperature is cold (low) and flow is high followed by a higher temperature in spring combined with less water. This process has been showed to be enhanced by the

ongoing climate warming through shortening or elimination of snow cover and glacial melt (FOEN (ed.), 2021; Michel et al., 2020; Van Vliet et al., 2013).

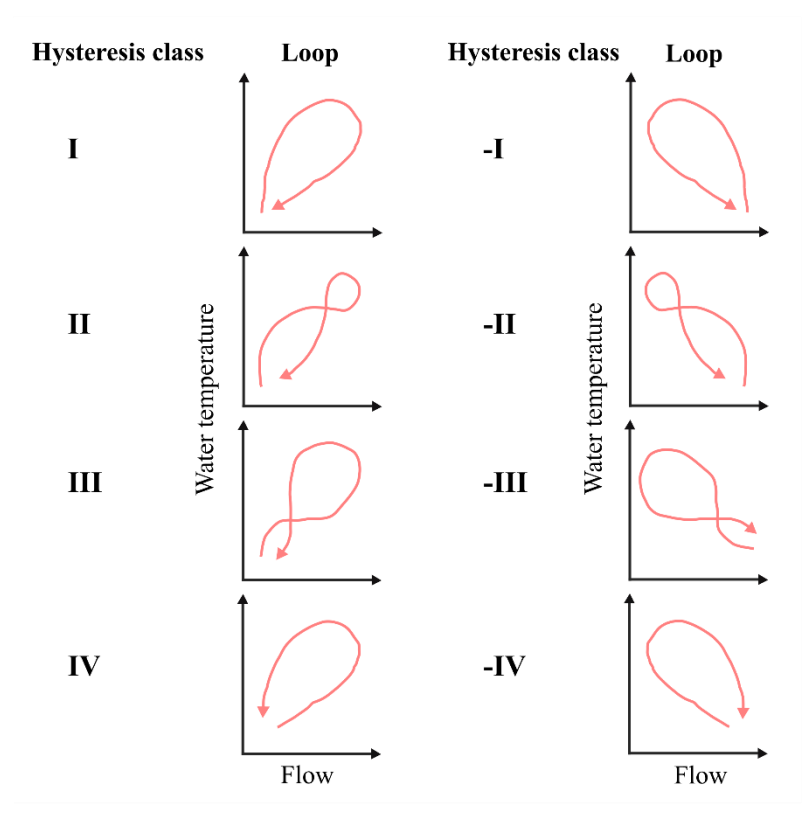


Figure 3. Hysteresis classes with corresponding hysteresis loops. Expanded with classes -I to -IV from Zuecco et al., (2016) to incorporate water temperature as the dependent variable.

To incorporate this reversed hysteretic loop, we added 4 *mirrored* hysteresis classes, -I to -IV, to the classes introduced by Zuecco et al., (2016) (Figure 3, right column). This was done by inverting the normalized flow prior to the computation of definite integrals, thus creating an increasing and decreasing independent variable. Note that the index works on set intervals. If the loops do not come back to their initial values, it works with open loops. The length of the data sets being investigated should depend on the quality and resolution of the data and the rate at which the dependent variable changes with respect to the independent variable (Zuecco et al., 2016). Here we used daily resolved datasets, averaged from 30 years of modeled data, thus always providing full annual loops.

2.8 Temperature extremes

Extreme conditions depend on what is considered to be extreme in relation to normal conditions (Stephenson, 2008). Here, water temperatures are considered to be extremely high if they exceed the 90th percentile during the 30-year reference, near- and far-future periods (IPCC, 2014).

We define a new *extreme event severity index*, as the temperature difference between the 90th percentile to the median for each climate simulation and period. If this temperature gap increases, it indicates that extreme temperatures become more severe as thermal peaks are elevated compared to the median temperature. *extreme event severity index* for each simulation and period is thus X °C from 0 °C, where X denotes the difference between the 90th percentile and the median temperature while 0 °C represent a match to the median temperature. Our analysis was made independent of when (beginning or end) in the 30-year periods it was conducted by removing the climatic trend for each simulation and period before calculating the

index. Note that by defining extreme events with the 90th percentile during each analyzed period, we consider temporal in-situ extreme events as they are experienced during the considered periods. We do not inflate our results by using past extreme event definitions to evaluate future extreme events.

2.9 Thermal thresholds for fish

By counting the number of days per year during which thermal thresholds are exceeded, effects of climate change on fish can be evaluated both locally and regionally (Michel et al., 2020). The occurrence of exceedance of specific river water temperature thresholds on a daily scale was used to investigate the historic past (1990 to 2019) and projected future (2070 to 2099) stress on the brown trout (*Salmo trutta*). Three thermal thresholds were chosen in order to incorporate important aspects in the life of the brown trout. including: (1) adult mortality as represented by a daily mean temperature above 25 °C (Elliott, 1981; Wehrly et al., 2007), also set as a hard upper limit for the thermal use of waters in Switzerland (Water Protection Ordinance 814.201); (2) an increased risk for proliferative kidney disease (PKD) as parasite activity as represented by a daily mean temperature above 15 °C (Chilmonczyk et al., 2002; Strepparava et al., 2018) and; (3) fish egg (roe) mortality from September to January as represented by a daily mean temperature above 13 °C (Elliott, 1981).

3 Results

3.1 Warming

The most influential factor for future river water temperatures are the climate change scenarios. Individual river water warming for the different stations, from the reference (1990-2019) to the near- (2030-2059) and far-future (2070-2099) periods, are shown in Figure 4. Under the RCP8.5 scenario, the warming of river temperatures increases throughout the 21st century, and even accelerates. The smallest change in river temperatures was observed under the RCP2.6 scenario, with warming reaching a plateau in the middle of the 21st century. The mean change in river temperatures from the reference period to the near- and far-future amounts to +0.77 and +0.91 °C for RCP2.6, to +0.95 and +1.51 °C for RCP4.5, and to +1.22 and +3.18 °C for RCP8.5, respectively. This amounts to an averaged water warming rate from 1990 to 2099 for RCP8.5 of 0.36 °C per decade, 0.19 °C per decade for RCP4.5, and 0.12 °C per decade for RCP2.6. At the same time as near-surface air temperature changed by 0.50 °C per decade for RCP3.5, 0.26 °C per decade for RCP4.5 and 0.13 °C per decade for RCP2.6.

Climate change impact was heterogeneous between stations, yet common patterns were found within thermal regimes (Figure 4, Table B8 in Appendix B). The strongest river water warming, regardless of climate scenario or time period, was observed for stations in the *Alpine* thermal regime, followed in order by *Downstream Lake*, *Regulated*, *Swiss Plateau*, and *Spring* thermal regimes. Under RCP8.5, river temperatures of *Alpine* stations, on average, warm by 1.44 °C until the near-future and by 3.54 °C until the far-future, compared to the reference period. The river water of *Downstream Lake* stations also strongly warmed, by 1.36 °C until the near-future and by 3.43 °C until the far-future. Compared to the *Alpine* and *Downstream Lake* thermal regimes, river temperatures of stations in the *Regulated* (near-future +1.19 °C, far-future +3.00 °C) and *Swiss Plateau* (near-future +1.06 °C, far-future +2.75 °C) thermal regimes warmed less. Least affected, by a wide margin, were the river temperatures of the 2 stations that classify as the *Spring* thermal regime (near-future +0.04 °C, far-future +0.10 °C).

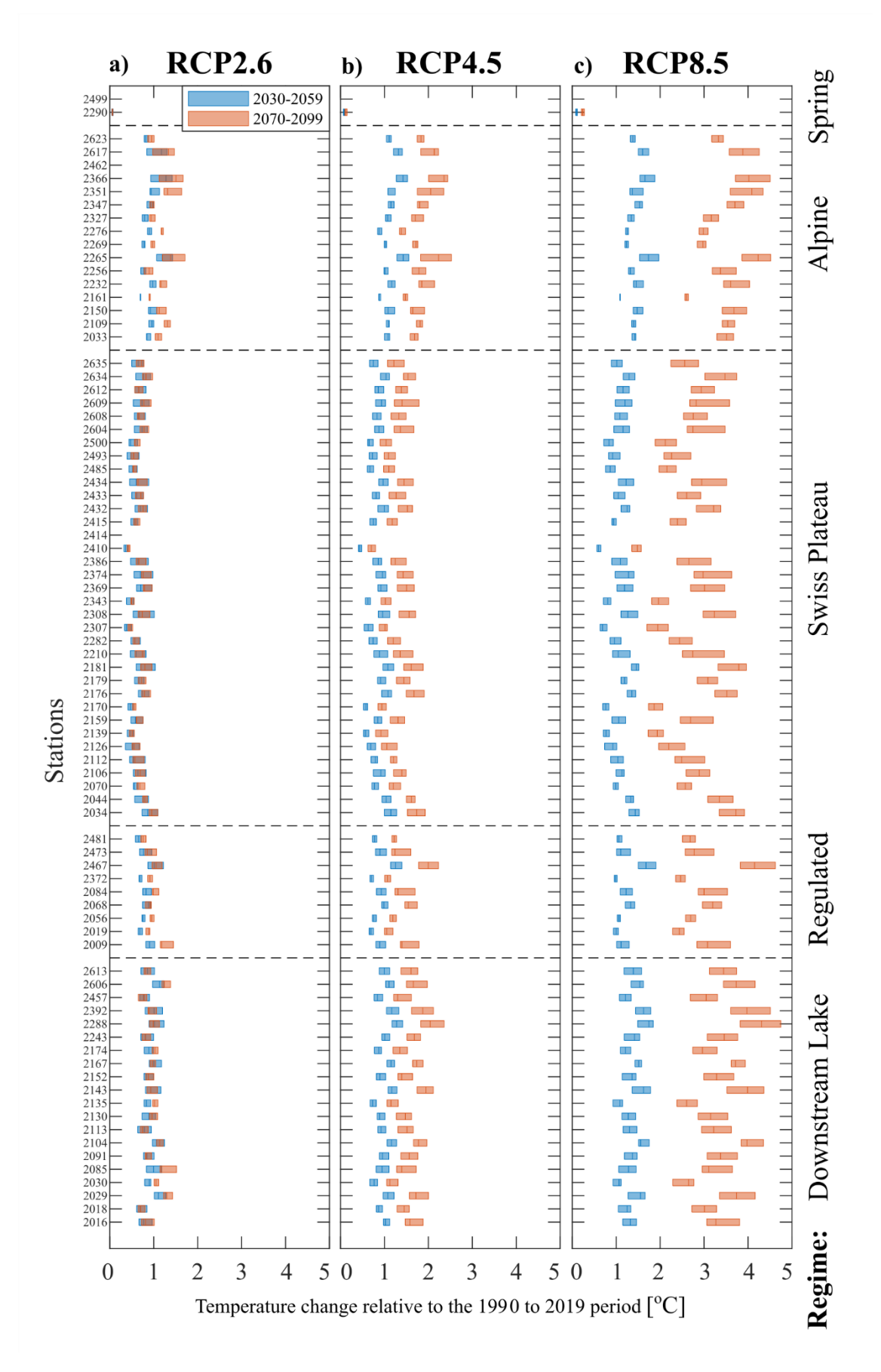


Figure 4. Modeled mean river temperature increase from the reference (1990 to 2019), to near-future (2030 to 2059, blue bars) and far-future (2070 to 2099, red bars) under climate scenarios RCP 2.6, RCP4.5 and RCP8.5. Shown is the median (bar center line) and the lower and upper quartiles (left and right bar extent) of the difference between periodic mean temperatures (over 30 years) for each available climate simulation additionally averaged where multiple hydrological models exist (M_1, M_2, M_3) , i.e., the bar extents show climate model variability in the mean temperature change between the three periods. Stations 2414 and 2462 are not shown since the flow model M_4 lacked 30 years of continuous data.

3.2 Hysteresis analysis

The hysteresis class could be determined for each station with future and present river discharge (47 out of 82 stations). For all stations, climate scenarios, and climate models, the index found solutions in hysteresis intervals ranging from 164 to 328 days. During the reference period the dominant hysteresis class was IV (45.6%) followed by III (25.0%), -I (14.7%), -II (11.8%) and I (2.9%) while no stations belonged to class II. For the reference period the classes remained independent in relation to the climate scenario (RCP8.5, 4.5, 2.6) or hydrological model (M₁, M₂, M₃) used, while in the near- and far-future differences start to show. For RCP8.5 in the far-future period the dominant class was -I (48.5%) followed by class IV (33.8%), III (13.2%) and -II (4.4%).

For the RCP8.5 scenario classes are shown for the reference, near- and far-future periods in Table 3 (hysteresis classes for RCP4.5 are shown in Table B9, and for RCP2.6 in Table B10, both in Appendix B). Under RCP8.5, the number of stations which changed hysteresis classes between the reference and the near-future was 23%, increasing to 51% until the far-future. Correspondingly, under RCP4.5, 23% had changed hysteresis classes when reaching the near-future, while 38% of the stations changed classes until the far-future. Under RCP2.6, 28% of stations had changed classes until the near-future, but once reaching the far-future, some stations changed back again and the fraction of stations that were in a different hysteresis class compared to the reference period was reduced to 21%.

Considering only the far-future period (2070 to 2099), stations belonging to the *Swiss Plateau* thermal regime showed the largest change in hysteresis loop classes, with 58% changing under RCP8.5, 42% under RCP4.5 and 12% under RCP2.6. Considering again only the far-future, stations belonging to the *Regulated* thermal regime exhibited hysteresis loop class changes of 50% under RCP8.5, 33% under RCP4.5 and 50% under RCP2.6. Least prone to hysteresis class changes in the far-future were stations of the *Alpine* thermal regime (38% under RCP8.5 and RCP4.5, 23% under RCP2.6). Out of the 20 *Downstream Lake* thermal regime stations only 2 stations were investigated with discharge (i.e. model with *air2stream* instead of *air2water*). From these 2 stations, 1 changed hysteresis class with RCP8.5 by the far-future, 1 with RCP2.6 but none with RCP4.5. As can be seen from 4 representative stations for the *Swiss Plateau*, *Regulated*, *Alpine*, and *Downstream Lake* illustrated in Figure 5, a change in hysteresis class is usually associated with a counterclockwise rotation and stretching of the loop from, for example a lower to a higher class (III to IV). Such rotation and stretching appears as a result of increased warming in summer combined with a decrease in summer discharge, while warming in winter is smaller than in summer and discharge is increasing.

Table 3. Modeled hysteresis classes during the reference (1990 to 2019), the near-future (2030 to 2059) and the far-future (2070 to 2099) periods for climate scenario RCP8.5. Flow data from models M₁, M₂ and M₃. Stations with no flow measurements for calibration, missing flow model output as forcing or where the use of the *air2water* model did not require flow as input have been excluded. A change in class from the reference period to the near- or far-future period is highlighted in *italic*. Classes are shown as natural numbers in stead of Roman numerals for ease of reading.

RCP8.5											
Station		eferen	ce		Near			Far			
	\mathbf{M}_{1}	M_2	M_3	\mathbf{M}_1	M_2	M_3	\mathbf{M}_{1}	M_2	M_3		
			Dow	nstrea	m Lak	e					
2016	4			4			-1				
2085	4		т	4 Regula	4-3		4				
2009	2		1	Keguia 4	tea		4				
2009	3	3		4	4		4	4			
2084		4		<i>'</i>	4		<i>'</i>	4			
2372	4	4		4	4		4	4			
2473	3	4	4	4	4	4	4	4	4		
2481		4		iss Pl		4	l .	4			
2034	-2	-2	511		-2		-2	-1			
2044	4	4	4	-2 -2	-1	-2	-1	-1	-1		
2070	4	4		4	4		-1	-1			
2106	-2	-2		-2	-2		-2	-1			
2112 2126		4 -1			4 -1			4 -1			
2159		4			4			-1 -1			
2176	4	4		4	4		-1	-1			
2179	4	4		4	4		-1	-1			
2181	4	4		4	4		-1	-1			
2210 2307	-1	-2 -1		-1	-2 -1		-1	-1 -1			
2307	-1	4		-1	-1 -1		-1	-1 -1			
2343		-1			-1			-1			
2369		-1			-1			-1			
2374		4			-1			-1			
2386 2415	2	-2 -2		2	-1 -2		2	-1 -1			
2413	-2 -1	-2 -1		-2 -1	-2 -1		-2 -1	-1 -1			
2434	1	-1		1	-1		1	-1			
2493		-1			-1			-1			
2500		-1			-1			-1			
2604 2609		4 4			4 4			- <i>1</i> 4			
2612		3			3			3			
2634		4	4		4	4		-1	-1		
				Alpir							
2033	3	3	2	4 4	4	1	4	4	4		
2109 2150	4		3	4		4	<i>4</i> 4		4		
2161	1		1	1		1	3		3		
2232	-	4	-		4	-	1	4	-		
2256	_	3		_	3		_	3			
2265	3		4	3		4	3		4		
2269 2276		4	4 4		4	4 4		4	4		
2327		7	3		7	3		7	3		
2351	3			4			4				
2366		3	3		4	4		4	3		
2617		3	3		3	3		3	3		

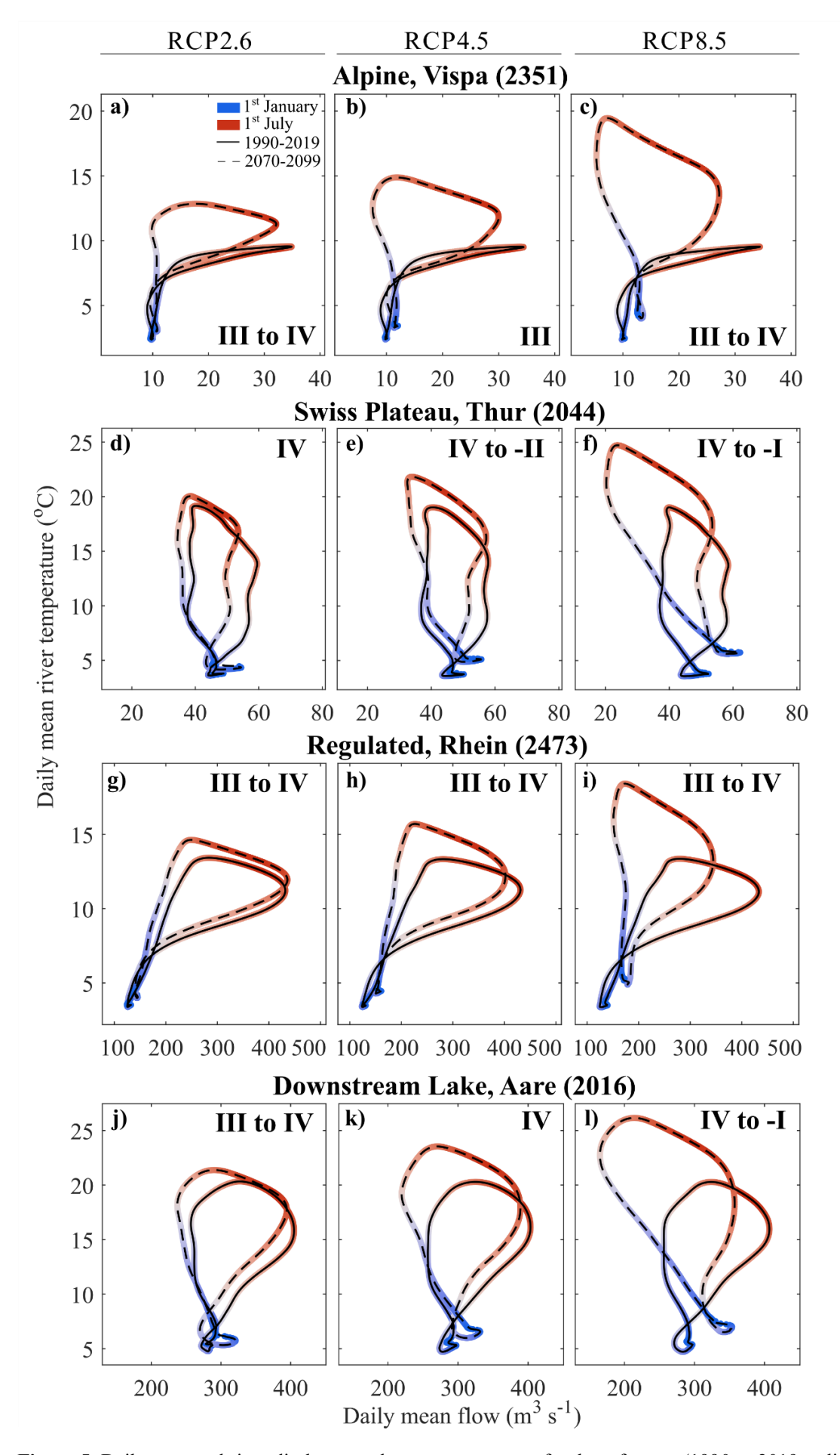


Figure 5. Daily averaged river discharge and water temperature for the reference (1990 to 2019, solid line) and the far-future period (2070 to 2099, dashed line) at 4 stations showing the current and the future thermal hysteresis loops. Flow data used is from model M₁, stations belong to the *Alpine*, *Swiss Plateau*, *Regulated* and *Downstream Lake* thermal regimes. Daily averaged datasets have been smoothed twice with a running average of 30 days. Hysteresis class change in roman numericals (cf. Fig. 4), station location in Fig. 2b.

3.3 Temperature extremes

The analysis is focused on temperature extremes in the summer months (June to August), during which the severity of extremes varies in between climate scenarios and is different on individual station basis and on a thermal regime basis (Figure 6). Note that the use of extreme event severity as an index should be viewed as the minimum temperature increase of extreme events in the future while it denotes the increase of the 90th percentile. From the reference (1990 to 2019) to the far-future (2070 to 2099) period the extreme event severity for scenario RCP2.6 increased on average by +0.20 °C (Figure 6a), by +0.38 °C for RCP4.5 (Figure 6 b) and by +0.61 °C for RCP8.5 (Figure 6 c).

Looking at extreme events at the level of thermal regimes, during the reference period (1990 to 2019), the most sever extreme temperatures occurred at stations in the *Swiss Plateau* and *Downstream Lake* thermal regimes. *Swiss Plateau* thermal regime (mean extreme event severity +2.8 °C) *Downstream Lake* (+2.2 °C), *Regulated* (+1.3 °C), *Alpine* (+1.1 °C) and *Spring* thermal regimes (+0.12 °C).

For all climate scenarios and all thermal regimes, the severity of extreme events increased throughout the 21st century. For the far-future (2070 to 2099), under all climate scenarios the Swiss Plateau and the Downstream Lake thermal regime stations remain as the stations with the severest extreme events, while the increase in extreme event severity increases the most for the Regulated and the Swiss Plateau thermal regimes. As the Swiss Plateau and Regulated thermal regime stations are mostly located in the Swiss low land in the Northwestern part of Switzerland (see Figure 2b), they are the ones that are expected to experience the most severe low flow conditions, especially in summer months under the RCP8.5 scenario, with a discharge reduction ranging from 5 to 60 % (FOEN, 2021; Brunner, et al., 2019; Brunner, et al., 2019; CH2018, 2018). The largest increase from the reference to the far-future period was found at stations for the Regulated thermal regime (mean extreme event severity increase RCP2.6: +0.28 °C, RCP4.5: +0.54 °C, RCP8.5: +0.93 °C) followed by the Swiss Plateau (RCP2.6: +0.26 °C, RCP4.5: +0.48 °C, RCP8.5: +0.78 °C), Alpine (RCP2.6: +0.23 °C, RCP4.5: +0.45 °C, RCP8.5: +0.68 °C), Downstream Lake (RCP2.6: +0.23 °C, RCP4.5: +0.40 °C, RCP8.5: +0.61 °C) and Spring thermal regimes (RCP2.6: +0.01 °C, RCP4.5: +0.01 °C, RCP8.5: +0.03 °C).

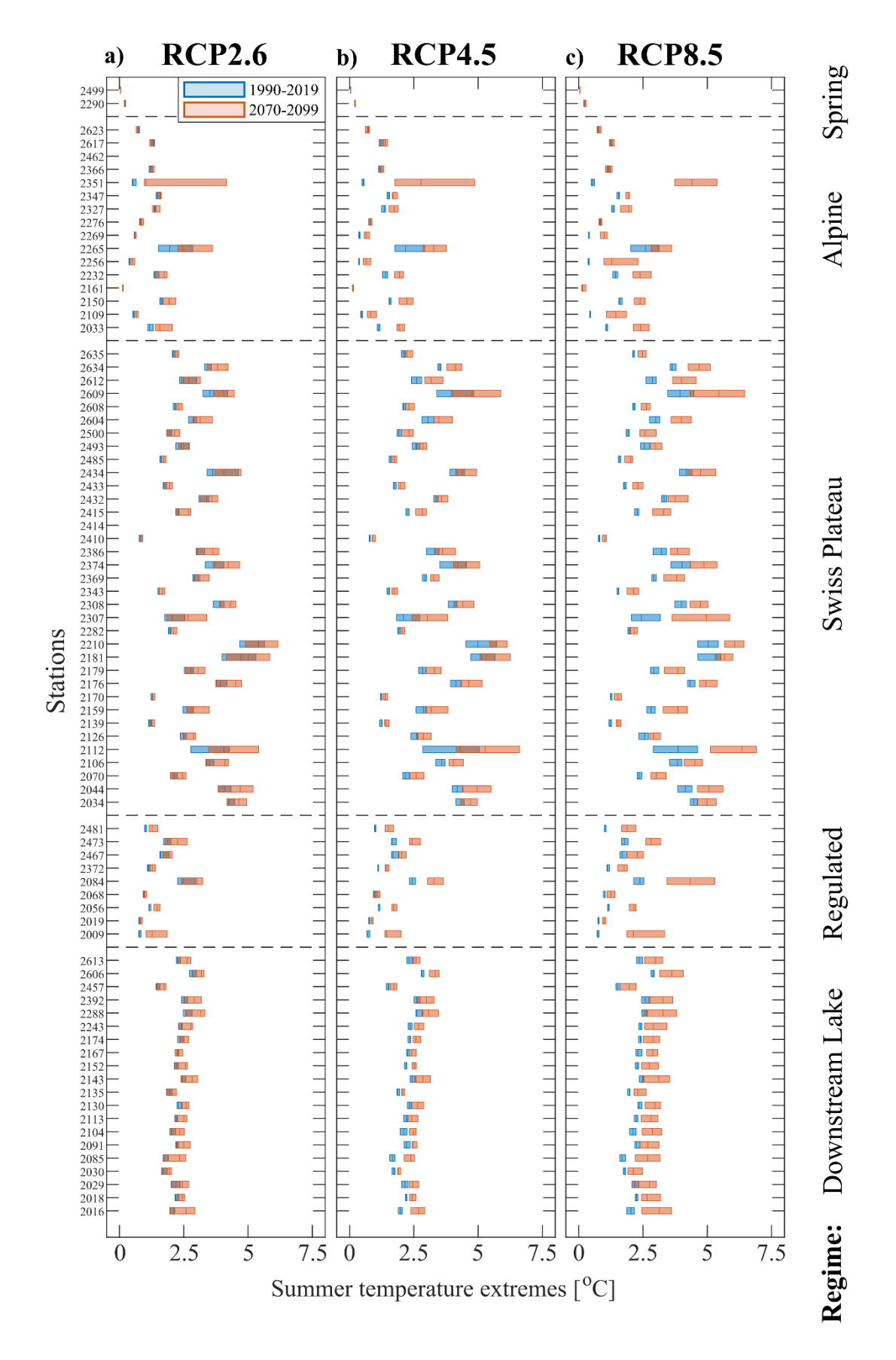


Figure 6. Severity of water temperature extremes from June to August for 30 years of climate simulations (blue bars 1990 to 2019, red bars 2070 to 2099) ordered according to thermal regime. Shown are the lower and upper quartiles (extent of bar) and the median (bar center line) of the difference between the 90th percentile to the seasonal median temperature (30 years of data) from all available climate models additionally averaged where multiple hydrological models exist (M_1 , M_2 , M_3) at each station and time period, i.e., the bar extents show climate model induced variability in each period. Stations 2414 and 2462 are not shown since the flow model M_4 lacked 30 years of continuous data.

3.4 Thermal thresholds

Our results show clear thermal regime dependent differences for the present and future thermal related stress on the brown trout (Figure 7). The lethal threshold (25 °C) was seldomly exceeded in the past (Figure 7a). However, towards the end of the 21st century, for a majority of stations in the *Downstream Lake* and *Swiss Plateau* thermal regimes the lethal threshold was exceeded on at least one day during the year, making areas which could previously be considered safe for the brown trout potentially lethal at least on certain days of the year. In addition, the 25 °C limit is also critical for anthropogenic water use in Switzerland, as the Swiss law (Water Protection Ordinance 814.201) prohibits a thermal use of waters for cooling purposes beyond this threshold. Unfortunately, our results not only show an increased occurrence of lethal temperatures, but also the less imminently lethal but nevertheless detrimental lower temperature threshold of the increased occurrence of the PKD disease (15 °C) will be exceeded much more frequently (see Figure 7b), as will the threshold for fish egg mortality (Figure 7c). Alpine, and to a lesser extend Regulated thermal regime stations, where previously the thermal conditions for an increased likelihood of PKD were not met, are likely also going to exhibit these conditions in the warmer summer months. Given the 153 days from September to January, egg development (approx. 30 to 90 days Alp et al., 2010) should still have enough time to take place safely throughout the 21st century in Regulated, Swiss Plateau, Alpine and Spring thermal regime rivers. Rivers in the Downstream Lake thermal regime are likely too large to facilitate spawning and were therefore not further considered in this analysis.

The results presented below represent the number of stations where the daily temperature was above a given thermal threshold (bar center line Figure 7 above 0). Under the RCP8.5 scenario from the reference to the far-future, the number of stations exceeding the mortality threshold (25 °C) increased from 4 to 37 stations from a total of 54 stations in the Downstream Lake and Swiss Plateau thermal regimes (Figure 7a). For the Regulated, Alpine and Spring thermal regime stations, none passed the lethal threshold during the reference period, but for the farfuture 1 out of 26 stations exceeded it. For Downstream Lake and Swiss Plateau thermal regime stations, the PKD threshold (15 °C) was largely exceeded already during the reference period (52 of 54 stations), increasing to all stations in the far-future (Figure 7b). For the Regulated, Alpine and Spring thermal regime stations, 2 out of 26 stations exceeded the PKD threshold already during the reference period. While in the far-future, 20 out of 26 Regulated, Alpine and Spring thermal regime stations broke through the 15 °C threshold. With respect to fish egg mortality (13 °C) from September to January, all Downstream Lake thermal regime stations exceeded this threshold both in the reference period as well as in the far-future (Figure 7c). During the reference period, 4 out of 9 Regulated and 31 out of 34 Swiss Plateau thermal regime stations exceeded the 13 °C threshold. Correspondingly, for the Regulated and Swiss Plateau thermal regimes, 8 out of 9 and all 34 stations, respectively, exceeded the 13 °C threshold during the far-future period. Although Alpine thermal regime stations never exceeded the 13 °C threshold during the reference period, 8 out of 16 stations exceeded this limit during the far-future period. From the two groundwater fed Spring stations, neither the mortality nor the PKD or fish egg mortality thresholds were exceeded.

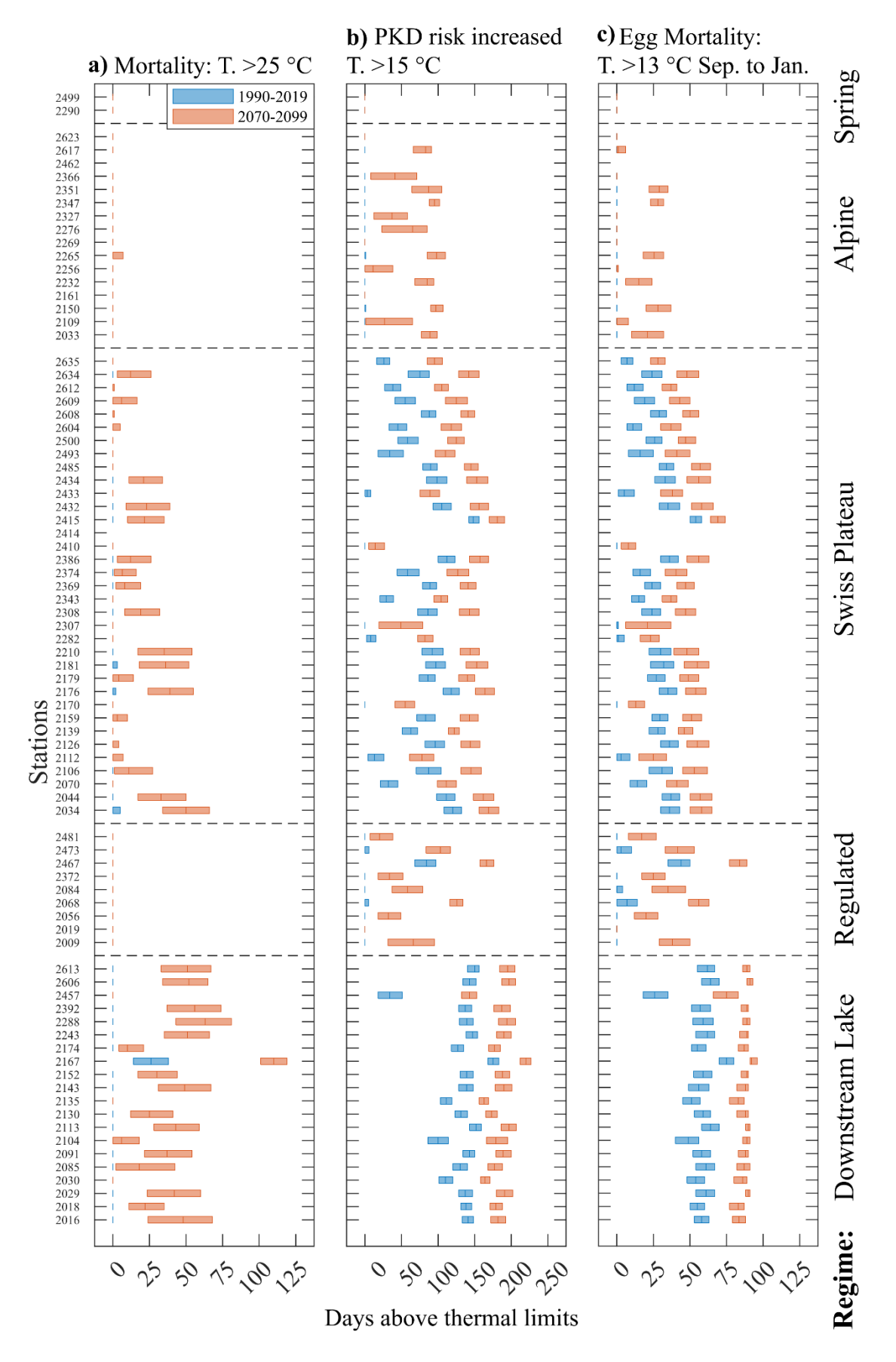


Figure 7. Number of days superseding thermal threshold for the brown trout for the RCP8.5 climate scenario. a) Mortality threshold at daily mean temperatures >25 °C, b) increased risk for proliferative kidney disease (PKD) at daily mean temperatures >15 °C, egg mortality during September to January at temperatures > 13 °C. Data consist of 30 years of climate simulations (blue bars 1990 to 2019, red bars 2070 to 2099) ordered according to thermal regime. Shown are the median (bar center line) and the lower and upper quartiles (left and right bar extent) of the climate simulation from all available climate models additionally averaged where multiple hydrological models exist (M_1 , M_2 , M_3), i.e., the bar extents show climate model induced variability for each period with annual resolution. Stations 2414 and 2462 are not shown since the flow model M_4 lacked 30 years of continuous data.

4 Discussion

4.1 Multi-fidelity modeling approach

The use of semi-empirical models by definition means that some of the physical processes affecting heating are simplified under parameterization and some are directly resolved. The models air2stream and air2water resolve the effect of river depth, discharge, thermal signals from tributaries, inverse stratification in lakes during winter, and seasonal cycles. The heat flux between the atmosphere and surface waters (latent and sensible heat, short and longwave radiation) is not directly resolved by air2stram and air2water. However, indirectly we consider climate related heat budget changes in our method, through the use of high-quality projections of air temperature and discharge as model input. Glacier retreat is included in the hydrological models providing discharge projections to this study (eg. Muelchi et al., 2021), however for temperature this effect is only indirectly considered in air2stream through reduced water availability in summer. The cooling effect on river water caused by meltwater from snow and ice does not change in our method, as snow and ice recede in a future climate it is expected that warming in high altitude rivers is larger than projected in this study. Therefore, if the relationships between discharge and air temperature towards water temperature remain similar in the future, our method can be used to reliably project future river temperatures. Importantly, the lower fidelity water temperature model approach used here combined with high-fidelity climate/hydrological model outputs as input enable the principle of multi-model ensemble, comparison and analysis that is required for robust climate change impact assessments (Duan et al., 2019).

To expand on previous results of river water temperature projections for Switzerland (Michel et al., 2022), we employed a multi-fidelity modeling approach able to automate the generation of water temperature simulators for the different national river temperature monitoring stations of Switzerland, as summarized in Figure 1. Models of varying complexity were built from integrating high-fidelity climate and hydrological modeling outputs (i.e., downscaled climate (Table 1) and hydrological model outputs (Figure 2a), CH2018 and Hydro-CH2018) with low-fidelity river temperature models of varying degrees of parametrization i.e., *air2water* and *air2stream* (Toffolon & Piccolroaz, 2015; Piccolroaz et al., 2013). Statistical learning-based coupling of atmospheric and hydrological stations (Table 2) and classification of river stations into thermal regimes (Figure 2b & 2c) enabled optimal low-fidelity model selection (Figure 2d) and parametrization.

4.2 Adjustment of trends

A trend bias correction was applied to the temperature model outputs due to the difference observed between modeled and measured trends (Table B3 to B6 in Appendix B). The correction decreased the difference between modeled and measured annual trends by approximately 0.1 °C per decade. After the bias correction, modeled annual trends with climate simulations as inputs followed closely the observed trends (Table B7 in Appendix B). Preadjustment climate scenarios have a different bias compared to measurements, with RCP8.5 simulations most closely following observed trends while RCP2.6 simulations exhibiting the largest bias. This discrepancy in bias is caused by the averaging of trends from either up to 22 (RCP8.5), 17 (RCP4.5) or 9 (RCP2.6) climate simulations. The trend bias adjustment was applied seasonally, resulting in an adjustment of 0.12 °C per decade on average. The largest adjustment was required for the June to August period (0.22 °C per decade) while the smallest adjustment was made for the December to February period (0.05 °C per decade). Note that only 2 out of 16 *Alpine* stations had long enough measured datasets (i.e., 30 years) to derive a historical trend, and that trend was used to adjust all 16 stations. The trend adjustment upscaled

from 2 to 16 *Alpine* stations, as well as the calibration at these stations, could thus benefit from longer time series; we therefore recommend care while using these bias corrected data. Additionally, for the groundwater fed station 2499 in the *Spring* thermal regime, measured water temperature is inversely correlated to air temperature. The result is a near zero or negative trend for the future (below 0 in Figure 4). Although the modeled trend at station 2499 is statistically significant, the result indicates a limitation in the *air2stream* model to resolve effectively groundwater dominated processes under climate change.

4.3 Warming rates, trends, and hysteresis analysis

As expected, the climate scenario turned out to be the most important factor for river water temperature increase. RCP8.5 being the scenario with the largest warming rate resulted in an average river water temperature increase of +3.2 °C (+0.36 °C per decade from 1990-2020 to 2070-2099) compared to +0.49 °C per decade warmer air temperatures. This is in agreement with previous findings for Swiss rivers, which projected a water temperature increase of up to +3.5 °C from 1990-2000 to 2080-2090 or +0.38 °C per decade (Michel et al., 2022) compared to a measured water temperature increase of +0.33 °C per decade from 1979 to 2018 (Michel et al., 2020) as well as for Swiss lake surface water temperatures, which were projected to increase by +3.3 °C from 1982–2010 to 2071-2099 (Råman Vinnå et al., 2021). In addition to the strong warming of water temperatures until the end of the century, the projections made herein also suggest that the seasonal patterns in the warming of near surface air temperatures in Switzerland are going to persist in river water temperatures, with stronger warming in summer compared to winter.

Among the different stations, common patterns and trends in river temperature warming could be identified by classifying the stations into the 4 different river thermal regimes occurring in Switzerland (Piccolroaz et al., 2016). The classification was further improved in this study by adding a groundwater spring class and using thermal pattern recognition to regroup river temperature monitoring stations by automatically identifying key thermal influences from upstream of a given monitoring station (e.g., the thermal influence of a lake, of tributaries or of a spring.

In terms of overall warming, the strongest warming on an annual basis emerged for stations in the *Alpine* thermal regime, followed, in order, by stations in the *Downstream Lake*, *Regulated*, *Swiss Plateau*, and *Spring* thermal regimes (Figure 4). The strong warming of *Alpine* regime stations has its origins in the strongest near-surface air temperature warming trend in summer that is occurring in southern parts of Switzerland (CH2018, 2018). The strong warming in the *Downstream Lake* thermal regime can be explained by the extended residence time of water in lakes compared to rivers in general (allowing longer time for waters to heat up) and to a difference in seasonal patterns, aspects that the employed *air2water* model explicitly considers. A previous coupled modeling study by the author showed that future lake surface waters (epilimnion) heat faster compared to river waters, with a difference in warming trends between Lake Biel and the Aare River of +0.03 °C per decade and between Lake Geneva and the Rhône River of +0.11 °C per decade (Råman Vinnå et al., 2018).

Finally, by using and extending an index developed for classifying hysteretic loops (Zuecco et al., 2016), it became apparent that climate warming adjust river temperature hysteresis towards a state with higher temperature and a river discharge decrease. This is seen as a stretching of most thermal loops diagonally towards the upper left (Figure 5). The trend stretching results from the general decrease in discharge as well as the increased seasonal near-surface air

temperature water warming occurring during the summer months. Together, these two processes predominantly increase water temperature in summer as well.

4.4 Thermal extremes

The here proposed *extreme event severity index* together with a removal of the climatic trend during each period, allowed us to investigate the change in the baseline of extreme temperature under each thermal regime considered here. The index is independent of past extreme conditions and relate extremes to the time period being investigated. Like for the water temperature warming rates and trends, the severity of temperature extremes was impacted the most by the choice of the climate scenario, similarly so for thermal regimes as a whole and for individual stations. The largest increase of river temperature extremes occurred under the RCP8.5 scenario, followed by the RCP4.5 scenario. Noteworthy is that under the RCP2.6 scenario, extreme event frequency and severity stayed more or less constant throughout the 21st century. As the discharge projections have been directly considered in the employed multifidelity modeling approach, the strong increase in extreme event severity for these stations is thus a direct result of the expected increased occurrence of low flow events, while the seasonal near-surface air temperature changes are mostly responsible for an increasing median of river water temperatures.

4.5 Thermal Thresholds

The likely impact of climate change under the RCP8.5 scenario was investigated with known thermal thresholds for the brown trout (i.e., risk of death at 25 °C and above; increased occurrence of PKD above 15 °C; increased fish egg mortality at 13 °C between September and January), a cold water fish species that is found in rivers and streams throughout all of Switzerland (Brodersen et al., 2023). While the brown trout can already die after about 10 min at temperatures of 30 °C (Elliott, 1981), due to the daily temporal resolution of the employed models, thermal thresholds could only evaluated on a daily time scale. Even when looking only at the daily time scale, the results of this study are cause for concern, as both the number of stations as well as the duration during which thermal thresholds are exceeded increase. Viewed alongside the fact that the number of catches of brown trout in Switzerland have already severely decreased in the past decades, for example from 73,500 in 1989 to 12,750 in 2019 in the rivers of the Swiss canton of Bern, which represents rivers of all types of thermal regimes that are found in Switzerland (FOEN, 2024), the outlook for the brown trout's future in Swiss rivers is grim.

The thermal analyses preformed here do not resolve all the processes affecting fishes' sensitivities to thermal extremes or spawning success. The ability to migrate, find local cold water refugia, or the availability for bottom gravel substrate required for spawning was not explicitly simulated. However, as severe temperature extremes which exceed the fish mortality threshold of 25 °C can in general occur in tandem with low flow conditions (see Figure 5), the possibilities for the brown trout to temporally migrate to a cold water refugia during such extremes can be expected to be strongly limited. And while we did not investigate the temperature to initiate spawning, it is likely that longer occurrence of high-water temperature periods during Autumn will have the potential to delay brown trout spawning. Moreover, due to increased river discharge and erosion in winter, sufficient bottom gravel substrate for spawning can be expected to decrease in future (Junker et al., 2015). Hence, to conclude, a changing climate will significantly increase the stress on brown trout, and given the widespread distribution of this fish species, future changes in temperature related death of adults cause us most concern.

5. Conclusions

An automated multi-fidelity modeling approach consisting of downscaled regional climate models, hydrological catchment models, and two semi-empirical water temperature models at variable degrees of parametrization complexity was used to investigate future river water temperatures across Switzerland under three climate scenarios. Model selection and performance was optimized by grouping river stations under thermal regimes using a process consisting of thermal pattern recognition with hierarchical clusters.

According to the simulations, for the high emission climate scenario (RCP8.5), average river water temperatures across Switzerland will increase by +3.2 °C (0.36 °C per decade from 2020 to 2099), while under the low emission scenario (RCP2.6) temperatures increase by only 0.9 °C. The strongest river water warming under the high emission scenario can be expected to occur in the Alpine thermal regime (+3.5 °C) followed by stations of the Downstream Lake thermal regime (+3.4 °C). A general shift in river discharge with less water in summer and more water in winter together with increased warming in summer produced increased seasonal warming which stretched hysteresis loops of water temperature versus discharge. The severity of thermal extremes in summer increased by, on average, 0.6 °C under the high emission scenario, while under the low emission scenario the increase was limited to 0.2 °C. Caused by future low flows, river stations in the Swiss Plateau thermal regime showed the most severe absolute river temperature extremes during the reference period, while the absolute extreme temperature change was largest of Regulated thermal regime stations (RCP2.6: +0.28 °C, RCP4.5: +0.54 °C, RCP8.5: +0.93 °C). Our results show increased future thermal stress on cold-water fish such as the brown trout, with substantial increases in the duration of threshold exceeding temperatures. These exceedances will lead to the increased likelihood of reproduction difficulties, occurrence of sickness and high temperature related mortality for brown trout in rivers where this previously was not a problem.

A multi-fidelity modeling approach was deemed necessary to work around computational limitations while investigating regional climate change across Switzerland. We show how surface water temperature models can be employed for various different thermal regimes by automatically adapting their parametrization complexity to the required level, including for stations downstream of lakes that are influenced strongly by the lake thermal regimes. Yet, future studies would benefit from connecting lakes and rivers in one modeling framework. The climate models used here were part of to the global CMIP5 and regional EUROCORDEX coordinated modeling efforts (CH2018, 2018). Future studies should however consider using the more recent CMIP6 or later collaborations for their projections.

Swiss water protection management leans on the sensitivity of species for enforcing thermal utility rules prohibiting thermal use past certain thresholds (Waters Protection Ordinance 814.201). Our results show a change in the duration and the location of threshold exceeding water temperatures, which threatens not only the brown trout but have implications for future anthropogenic use of Swiss surface waters. Local and regional climate protection measures to limit negative effects of climate change includes but are not limited to the creation of river bank shading (Trimmel et al., 2018), dam management (Payne et al., 2004), river restoration, stormwater and site-specific management (Palmer et al., 2008) as well as managed ground water recharge (Epting et al., 2023). Ultimately to mitigate negative climate impact, management needs to weigh the need for protection and preservation with its associated cost and benefit towards the outcome of a non-interactive, partial or full climate protection approach.

Data availability

Atmospheric temperature climate data from the CH2018 project was obtained from the Swiss National Centre for Climate Services (nccs.admin.ch) data portal. On the same portal, discharge datasets from the Hydro-CH2018 project are available but at a temporally limited scale (monthly, seasonally and yearly means). We required daily resolved discharge data which was obtained directly from Massimiliano Zappa (model M₁), Daphné Freudiger (M₃), and Adrien Michel (M₄). Data from model M₂ (Muelchi et al., 2021) is available at http://doi.org/10.5281/zenodo.3937485. All modeled water temperature results for GCM-RCMs analyzed and left out (Table 1) and bias corrected input datasets of air temperature and discharge produced here are publicly available at http://doi.org/10.5281/zenodo.16967946.

Author contributions

LRV and JE came up with the concept and secured the funding. VB designed and performed the thermal pattern recognition, VB and LRV implemented it for ordering catchments according to thermal regimes. LRV conducted the forcing data adjustment, model setup and use. LRV and JE conducted the analysis of the results. OS provided scientific support. All authors took part in the writing of this manuscript.

Acknowledgments

We acknowledge the support from Martin Schmid for external scientific quality control, Amber van Hamel for valuable insights in the thermal extreme analysis, Sebastiano Piccolroaz for guidance in the use of the *air2stream* and the *air2water* models, Thilo Herold at the Swiss Federal Office of the Environment (FOEN) for project support and the Freiwillige Akademische Gesellschaft (FAG) Basel for funding this work.

Competing interests

The authors declare no competing interests.

References

- Alp, A., Erer, M., & Kamalak, A. (2010). Eggs Incubation, Early Development and growth in Frys of Brown Trout (Salmo trutta macrostigma) and Black Sea Trout (Salmo trutta labrax). *Turkish Journal of Fisheries and Aquatic Sciences*, 10(3). https://doi.org/10.4194/trjfas.2010.0312
- Barbarossa, V., Bosmans, J., Wanders, N., King, H., Bierkens, M. F. P., Huijbregts, M. A. J., & Schipper, A. M. (2021). Threats of global warming to the world's freshwater fishes. *Nature Communications*, 12(1), 1701. https://doi.org/10.1038/s41467-021-21655-w
- Benyahya, L., Caissie, D., St-Hilaire, A., Ouarda, T. B. M. J., & Bobée, B. (2007). A Review of Statistical Water Temperature Models. *Canadian Water Resources Journal*, 32(3), 179–192. https://doi.org/10.4296/cwrj3203179
- Birsan, M.-V., Molnar, P., Burlando, P., & Pfaundler, M. (2005). Streamflow trends in Switzerland. *Journal of Hydrology*, 314(1–4), 312–329. https://doi.org/10.1016/j.jhydrol.2005.06.008
- Bögli, R. (2020). *Time Series Clustering with Water Temperature Data*. University of applied sciences and arts Northwestern Switzerland (FHNW).
- Brodersen, J., Hellmann, J., & Seehausen, O. (2023). Erhebung der Fischbiodiversität in Schweizer Fliessgewässern. Progetto Fiumi Schlussbericht. Eawag: Swiss Federal Institute of Aquatic Science and Technology. https://doi.org/10.55408/eawag:30020
- Brunner, M. I., Farinotti, D., Zekollari, H., Huss, M., & Zappa, M. (2019). Future shifts in extreme flow regimes in Alpine regions. *Hydrology and Earth System Sciences*, 23(11), 4471–4489. https://doi.org/10.5194/hess-23-4471-2019
- Brunner, M. I., Björnsen Gurung, A., Zappa, M., Zekollari, H., Farinotti, D., & Stähli, M. (2019).

 Present and future water scarcity in Switzerland: Potential for alleviation through reservoirs and lakes. *Science of The Total Environment*, 666, 1033–1047. https://doi.org/10.1016/j.scitotenv.2019.02.169
- CH2018. (2018). CH2018 Climate Scenarios for Switzerland, Technical Report, National Centre for Climate Services, Zurich, 271 pp. ISBN: 978-3-9525031-4-0.
- CH2018 Project Team (2018): CH2018 Climate Scenarios for Switzerland. National Centre for Climate Services. doi: 10.18751/Climate/Scenarios/CH2018/1.0. (n.d.). [Data set].
- Chilmonczyk, S., Monge, D., & De Kinkelin, P. (2002). Proliferative kidney disease: cellular aspects of the rainbow trout, *Oncorhynchus mykiss* (Walbaum), response to parasitic infection. *Journal of Fish Diseases*, 25(4), 217–226. https://doi.org/10.1046/j.1365-2761.2002.00362.x

- Crank, J., & Nicolson, P. (1947). A practical method for numerical evaluation of solutions of partial differential equations of the heat-conduction type. *Mathematical Proceedings of the Cambridge Philosophical Society*, *43*(1), 50–67. https://doi.org/10.1017/S0305004100023197
- Diaz-Nieto, J., & Wilby, R. L. (2005). A comparison of statistical downscaling and climate change factor methods: impacts on low flows in the River Thames, United Kingdom. *Climatic Change*, 69(2–3), 245–268. https://doi.org/10.1007/s10584-005-1157-6
- Duan, H., Zhang, G., Wang, S., & Fan, Y. (2019). Robust climate change research: a review on multi-model analysis. *Environmental Research Letters*, 14(3), 033001. https://doi.org/10.1088/1748-9326/aaf8f9
- Elliott, J. M. (1981). Some aspects of thermal stress on fresh-water teleosts. Stress Fish 209–245.
- Elliott, J. M. (1994). Quantitative Ecology and the Brown Trout. Oxford series in ecology and evolution,

 Band 7. Oxford University Press: 286. ISSN: 1746-3130.
- Epting, J., Råman Vinnå, L., Annette, A., Stefan, S., & Schilling, O. S. (2023). Climate change adaptation and mitigation measures for alluvial aquifers Solution approaches based on the thermal exploitation of managed aquifer (MAR) and surface water recharge (MSWR). *Water Research*, 238, 119988. https://doi.org/10.1016/j.watres.2023.119988
- Fernández-Godino, M. G. (2023). Review of multi-fidelity models. *Advances in Computational Science* and Engineering, 1(4), 351–400. https://doi.org/10.3934/acse.2023015
- Ficklin, D. L., Hannah, D. M., Wanders, N., Dugdale, S. J., England, J., Klaus, J., et al. (2023).

 Rethinking river water temperature in a changing, human-dominated world. *Nature Water*,

 1(2), 125–128. https://doi.org/10.1038/s44221-023-00027-2
- FOEN. (2024). Catch statistics of Switzerland, Swiss Federal Office of Environment FOEN, Bern, Switzerland. URL: https://www.fischereistatistik.ch/.
- FOEN (ed.). (2021). Effects of climate change on Swiss water bodies. Hydrology, water ecology and water management. Federal Office for the Environment FOEN, Bern. Environmental Studies No. 2101: 125 p.
- Freudiger, D., Vis, M., & Seibert, J. (2021). Quantifying the contributions to discharge of snow and glacier melt. Hydro-CH2018 project. Commissioned by the Federal Office for the Environment (FOEN), Bern, Switzerland, 49 pp.

- Gharari, S., & Razavi, S. (2018). A review and synthesis of hysteresis in hydrology and hydrological modeling: Memory, path-dependency, or missing physics? *Journal of Hydrology*, *566*, 500–519. https://doi.org/10.1016/j.jhydrol.2018.06.037
- Guse, B., Fatichi, S., Gharari, S., & Melsen, L. A. (2021). Advancing Process Representation in Hydrological Models: Integrating New Concepts, Knowledge, and Data. Water Resources Research, 57(11). https://doi.org/10.1029/2021wr030661
- Hari, R., & Güttinger, H. (2004). Temperaturverlauf in Schweizer Flüssen 1978 bis 2002–

 Auswertungen und grafische Darstellungen fischrelevanter Parameter (No. Teilprojekt 01/08).

 Fischnetz-Publikation, Eawag, Dübendorf, Switzerland.
- Hari, R. E., Livingstone, D. M., Siber, R., Burkhardt-Holm, P., & Guettinger, H. (2006). Consequences of climatic change for water temperature and brown trout populations in Alpine rivers and streams. *Global Change Biology*, *12*, 10–26. https://doi.org/10.1111/j.1365-2486.2005.01051.x
- IPCC. (2014). Climate Change 2014: Synthesis Report. Contribution of Working Groups I, II and III to the Fifth Assessment Report of the Intergovernmental Panel on Climate Change [Core Writing Team, R.K. Pachauri and L.A. Meyer (eds.)]. IPCC, Geneva, Switzerland, 151 pp.
- Junker, J., Heimann, F. U. M., Hauer, C., Turowski, J. M., Rickenmann, D., Zappa, M., & Peter, A. (2015). Assessing the impact of climate change on brown trout (Salmo trutta fario) recruitment. Hydrobiologia, 751(1), 1–21. https://doi.org/10.1007/s10750-014-2073-4
- Kennedy, J., & Eberhart, R. (1995). Particle swarm optimization. In *Proceedings of ICNN'95 International Conference on Neural Networks* (Vol. 4, pp. 1942–1948). Perth, WA, Australia: IEEE. https://doi.org/10.1109/ICNN.1995.488968
- La Fuente, S., Jennings, E., Gal, G., Kirillin, G., Shatwell, T., Ladwig, R., et al. (2022). Multi-model projections of future evaporation in a sub-tropical lake. *Journal of Hydrology*, 128729. https://doi.org/10.1016/j.jhydrol.2022.128729
- Leach, J. A., & Moore, R. D. (2019). Empirical Stream Thermal Sensitivities May Underestimate Stream Temperature Response to Climate Warming. *Water Resources Research*, *55*(7), 5453–5467. https://doi.org/10.1029/2018WR024236
- Meehl, G. A., Stocker, T. F., Collins, W. D., Friedlingstein, P., Gaye, A. T., Gregory, J. M., et al. (2007).

 Global Climate Projections. In: Climate Change 2007: The Physical Science Basis.

 Contribution of Working Group I to the Fourth Assessment Report of the Intergovernmental

 Panel on Climate Change [Solomon, S., D. Qin, M. Manning, Z. Chen, M. Marquis, K.B. Averyt,

- M. Tignor and H.L. Miller (eds.)]. Cambridge University Press, Cambridge, United Kingdom and New York, NY, USA.
- Michel, A., Brauchli, T., Lehning, M., Schaefli, B., & Huwald, H. (2020). Stream temperature and discharge evolution in Switzerland over the last 50 years: annual and seasonal behaviour. Hydrology and Earth System Sciences, 24(1), 115–142. https://doi.org/10.5194/hess-24-115-2020
- Michel, A., Schaefli, B., Wever, N., Zekollari, H., Lehning, M., & Huwald, H. (2022). Future water temperature of rivers in Switzerland under climate change investigated with physics-based models. *Hydrology and Earth System Sciences*, 26(4), 1063–1087. https://doi.org/10.5194/hess-26-1063-2022
- Minville, M., Brissette, F., & Leconte, R. (2008). Uncertainty of the impact of climate change on the hydrology of a nordic watershed. *Journal of Hydrology*, 358(1–2), 70–83. https://doi.org/10.1016/j.jhydrol.2008.05.033
- Misset, C., Recking, A., Legout, C., Poirel, A., Cazilhac, M., Esteves, M., & Bertrand, M. (2019). An attempt to link suspended load hysteresis patterns and sediment sources configuration in alpine catchments. *Journal of Hydrology*, *576*, 72–84. https://doi.org/10.1016/j.jhydrol.2019.06.039
- Muelchi, R., Rössler, O., Schwanbeck, J., Weingartner, R., & Martius, O. (2021). An ensemble of daily simulated runoff data (1981–2099) under climate change conditions for 93 catchments in Switzerland (Hydro-CH2018-Runoff ensemble). *Geoscience Data Journal*, gdj3.117. https://doi.org/10.1002/gdj3.117
- Nicolle, P., Besson, F., Delaigue, O., Etchevers, P., François, D., Le Lay, M., et al. (2020).

 PREMHYCE: An operational tool for low-flow forecasting. *Proceedings of the International Association of Hydrological Sciences*, 383, 381–389. https://doi.org/10.5194/piahs-383-381-2020
- Palmer, M. A., Reidy Liermann, C. A., Nilsson, C., Flörke, M., Alcamo, J., Lake, P. S., & Bond, N. (2008). Climate change and the world's river basins: anticipating management options. Frontiers in Ecology and the Environment, 6(2), 81–89. https://doi.org/10.1890/060148
- Payne, J. T., Wood, A. W., Hamlet, A. F., Palmer, R. N., & Lettenmaier, D. P. (2004). Mitigating the Effects of Climate Change on the Water Resources of the Columbia River Basin. *Climatic Change*, 62(1–3), 233–256. https://doi.org/10.1023/B:CLIM.0000013694.18154.d6

- Piccolroaz, S., Toffolon, M., & Majone, B. (2013). A simple lumped model to convert air temperature into surface water temperature in lakes. *Hydrology and Earth System Sciences*, *17*(8), 3323–3338. https://doi.org/10.5194/hess-17-3323-2013
- Piccolroaz, Sebastiano. (2016). Prediction of lake surface temperature using the air2water model: guidelines, challenges, and future perspectives. *Advances in Oceanography and Limnology*, 7(1). https://doi.org/10.4081/aiol.2016.5791
- Piccolroaz, Sebastiano, Calamita, E., Majone, B., Gallice, A., Siviglia, A., & Toffolon, M. (2016).

 Prediction of river water temperature: a comparison between a new family of hybrid models and statistical approaches. *Hydrological Processes*, 30(21), 3901–3917. https://doi.org/10.1002/hyp.10913
- Råman Vinnå, L., Wüest, A., Zappa, M., Fink, G., & Bouffard, D. (2018). Tributaries affect the thermal response of lakes to climate change. *Hydrol. Earth Syst. Sci.*, 22, 31–51. https://doi.org/10.5194/hess-22-31-2018
- Råman Vinnå, Love, Medhaug, I., Schmid, M., & Bouffard, D. (2021). The vulnerability of lakes to climate change along an altitudinal gradient. *Communications Earth & Environment*, 2(1), 35. https://doi.org/10.1038/s43247-021-00106-w
- Schewe, J., Heinke, J., Gerten, D., Haddeland, I., Arnell, N. W., Clark, D. B., et al. (2014). Multimodel assessment of water scarcity under climate change. *Proceedings of the National Academy of Sciences*, 111(9), 3245–3250. https://doi.org/10.1073/pnas.1222460110
- Shen, H., Tolson, B. A., & Mai, J. (2022). Time to Update the Split-Sample Approach in Hydrological Model Calibration. *Water Resources Research*, *58*(3). https://doi.org/10.1029/2021WR031523
- Stephenson, D. B. (2008). Definition, diagnosis, and origin of extreme weather and climate events. In H. F. Diaz & R. J. Murnane (Eds.), *Climate Extremes and Society* (1st ed., pp. 11–23). Cambridge University Press. https://doi.org/10.1017/CBO9780511535840.004
- Strepparava, N., Segner, H., Ros, A., Hartikainen, H., Schmidt-Posthaus, H., & Wahli, T. (2018).

 Temperature-related parasite infection dynamics: the case of proliferative kidney disease of brown trout. *Parasitology*, *145*(3), 281–291. https://doi.org/10.1017/S0031182017001482
- Tananaev, N. I. (2012). Hysteresis effect in the seasonal variations in the relationship between water discharge and suspended load in rivers of permafrost zone in Siberia and Far East. *Water Resources*, 39(6), 648–656. https://doi.org/10.1134/S0097807812060073

- Toffolon, M., & Piccolroaz, S. (2015). A hybrid model for river water temperature as a function of air temperature and discharge. *Environmental Research Letters*, 10(11), 114011. https://doi.org/10.1088/1748-9326/10/11/114011
- Toffolon, M., Piccolroaz, S., Majone, B., Soja, A.-M., Peeters, F., Schmid, M., & Wüest, A. (2014).

 Prediction of surface temperature in lakes with different morphology using air temperature.

 Limnology and Oceanography, 59(6), 2185–2202. https://doi.org/10.4319/lo.2014.59.6.2185
- Trimmel, H., Weihs, P., Leidinger, D., Formayer, H., Kalny, G., & Melcher, A. (2018). Can riparian vegetation shade mitigate the expected rise in stream temperatures due to climate change during heat waves in a human-impacted pre-alpine river? *Hydrology and Earth System Sciences*, 22(1), 437–461. https://doi.org/10.5194/hess-22-437-2018
- Van Vliet, M. T. H., Ludwig, F., Zwolsman, J. J. G., Weedon, G. P., & Kabat, P. (2011). Global river temperatures and sensitivity to atmospheric warming and changes in river flow. *Water Resources Research*, 47(2), 2010WR009198. https://doi.org/10.1029/2010WR009198
- Van Vliet, Michelle T. H., Thorslund, J., Strokal, M., Hofstra, N., Flörke, M., Ehalt Macedo, H., et al. (2023). Global river water quality under climate change and hydroclimatic extremes. *Nature Reviews Earth & Environment*, 4(10), 687–702. https://doi.org/10.1038/s43017-023-00472-3
- Van Vliet, Michelle T.H., Franssen, W. H. P., Yearsley, J. R., Ludwig, F., Haddeland, I., Lettenmaier, D. P., & Kabat, P. (2013). Global river discharge and water temperature under climate change.

 Global Environmental Change*, 23(2), 450–464.

 https://doi.org/10.1016/j.gloenvcha.2012.11.002
- Webb, B. W., & Nobilis, F. (1994). Water temperature behaviour in the River Danube during the twentieth century. *Hydrobiologia*, 291(2), 105–113. https://doi.org/10.1007/BF00044439
- Wehrly, K. E., Wang, L., & Mitro, M. (2007). Field-Based Estimates of Thermal Tolerance Limits for Trout: Incorporating Exposure Time and Temperature Fluctuation. *Transactions of the American Fisheries Society*, 136(2), 365–374. https://doi.org/10.1577/T06-163.1
- WMO Guidelines on the Calculation of Climate Normals. (2017).
- Zuecco, G., Penna, D., Borga, M., & Van Meerveld, H. J. (2016). A versatile index to characterize hysteresis between hydrological variables at the runoff event timescale. *Hydrological Processes*, 30(9), 1449–1466. https://doi.org/10.1002/hyp.10681